Printable surface hologram via nanosecond laser ablation

by

Qiancheng Zhao

A thesis submitted to the University of Birmingham

for the degree of

MSc by Research

School of Mechanical Engineering

The University of Birmingham

January 2016

Supervisor: Carl Anthony

Co supervisor: Haider Butt

Abstract

Holography plays a significant role in applications such as data storage, light trapping, security, and biosensors. However, traditional fabrication methods remain time-consuming, labour-intensive, complex and costly, limiting the extensive and massive production of holograms. In this thesis, a single-pulse laser ablation strategy was used to write surface gratings and Fresnel zone plates. A 5 ns high-energy green laser pulse was utilized to form interference patterns on ink-based (150 nm thickness) and gold-based (4 nm thickness) substrates. The holographic recording process was completed within seconds. The periodicities for ink-based and gold-based gratings are 2.6 μm and 820 nm, respectively. The optical characteristics of the interference patterns have been computationally modelled, and well-ordered diffraction patterns were observed from the fabricated grating holograms by different monochromatic wavelengths. In addition, the asymmetric zone plate was fabricated on 4.5 nm gold layer, and a well-ordered rainbow pattern with a significant diffraction angle of 32 ° was measured from the normal incident for the focal point. An optical power meter experiment was also conducted to determine the diffraction efficiency of 0.8% by white light illumination. Personalised handwritten signatures and 3D coin images were further demonstrated to support the utilization of single laser ablation approach, and the fabrication methodology holds great potential in applications for optical devices.

Acknowledgements

First of all, I would like to express my sincere gratitude and great respect to my supervisor Carl Anthony who supported me all the way during my master research period. His kind and generous guidance helped me to go through the difficulties and encouraged me to be active and creative during my research.

I would like to thank my co-supervisor Haider butt for his comprehensive knowledge and fruitful suggestions, thanks for his great patience and insightful comments during my progress. I would also like to thank my college Aydin Sabouri who assisted me with my experiments and gave me useful advices.

The assistance and support from all my colleagues in micro-engineering group are highly appreciated during my research time. In addition, thanks to my friends in Birmingham to give me accompany and energy all the way up.

Last but not at least, I would show my great thankfulness to my beloved parents, Yingzhen Zheng and Zhijun Zhao, they always give me continuous support and selfless caring which push me ahead to finish my research firmly and steadily.

CONTENTS

List of Figures

List of Tables

ABBREVIATIONS AND ACRONYMS

VPH	Volume Phase Hologram
VHG	Volume Holographic Grating
SHSG	Silver Halide Sensitive Gelatin
DLIP	Direct Laser Interference Patterning
PMMA	Polymethyl Methacrylate
SEM	Scanned Electronic Microscope
AFM	Atomic Force Microscope
FEM	Finite Element Method
NA	Numerical Aperture

1. Introduction

1.1 Overall Aim and Objectives of Thesis

The overall project is fully supported and funded under Philip Leverhulme Trust 2013, to advance the research for nanofabrication on hologram production. Holograms have attracted scholars and researchers' interest and attention for their superior characteristics such as data storage, reproduction of original light field, security identification and biosensors. In the early 1940s, Dennis Gabor from British invented the electron holography when he built on pioneering work the field of X-ray microscopy. However, the first laser enabled optical hologram was created by Yuri Denisyuk in the Soviet Union in 1962 [1]. So far, a diversity of methodologies have been developed to fabricate holograms. Nevertheless, most fabrication strategies remain costly and labour-intensive. Taking multibeam interference technology [2-5] as an example, it requires precise interferometric alignment of laser beams from beam-splitting and focusing system. In this case, the preparation work is time-consuming and it limits the use of 3D holographic recording due to remarkable laser energy decrease and misalignment of laser splitter system. Therefore, developing an inexpensive, rapid and time-saving hologram fabrication approach remains challenging and significant.

The main objective of the research from the project is to develop a simple, rapid, economic and labour-saving fabrication method to record surface hologram. The

overall target is composed of different individual parts. Firstly, the selection of recording material for surface hologram needs to be discreet. Appropriate material can result in good performance of diffraction for holograms (e.g. good resolution limit to fully resolve the interference fringes to achieve high diffraction intensity). Subsequently, the recording system of hologram should be refined and easy to control as it is directly related to the formation of a surface hologram. Additionally, computational simulation regarding interference pattern of coherent beams are necessary for prediction of potential holograms, which may in turn affect the configuration of laser system. Finally, a series of optical experiment should be conducted to assess the diffraction characteristics for designed hologram.

Based on primary purpose of research in this project, the following objectives should be outlined and fulfilled to record surface holograms through nanofabrication:

1. To do comprehensive and considerable literature review on holograms, including the definition, classification, and fabrication methods, to discuss the advantages and limitations of current fabrication approaches.

2. To propose a scheme and fabrication strategy for preparation of surface hologram.

3. To figure out theoretical equations according to interference of laser beams. To demonstrate computational simulation in line with light field interference.

4. To measure and characterize the features of ablated holograms, including the morphology and optical characterization for hologram samples.

5. To discuss the experimental results (diffraction angle, diffraction efficiency)

with regards to target holographic samples; To compare simulated results with the experimental data, and analyse possible errors and distinctions between these two means.

1.2 Thesis Structure and Organisation

In this thesis, five chapters are constructed and organised. The first chapter introduces the overall research objectives and outlines the structure for whole paper. In the second chapter, the definition and classification of holograms, background and development of hologram, diversity hologram recording technologies are presented and summarised in detail and through comprehensive and intensive literature review, a hologram fabrication strategy is proposed and utilized in Chapter 3. An ink-based grating sample is made *via* this methodology. In addition, computational simulation of intensity distribution by coherent laser beams interference is conducted. Furthermore, a series of optical microscopy images are taken to characterize the fabricated holograms. In Chapter 4,gold-based holographic samples are prepared and a series of optical experiments are performed to characterize ablated holograms, including angular-resolved power meter and spectrometer measurements. The experimental data are processed to evaluate the diffraction characteristics. Further 3D holograms including polychrome coin hologram and handwritten ink hologram are demonstrated to stretch the application of laser beam interference. Chapter 5 discusses the advantages and limitations of proposed holographic fabrication strategy, a variety of future work and applications are proposed corresponding to this nanosecond laser

fabrication technique. Some future work and recommendations are included finally to advance the holographic fabrication system.

2. Literature Review

2.1 Introduction of Holography

The first holographic technology was discovered and invented by British researcher Dennis Gabor in 1940s by an unexpected result from X-ray electron microscope experiment [6, 7], it is known as electron holography. However, the real sense of optical hologram didn't come out until Soviet Union scientist Denisyuk [1] firstly enabled image recording of three dimensional objects to obtain information in amplitude, phase and spectral characteristics of object beam. Such recording media can reproduce virtual object and the original light field can be reconstructed by illumination of white light. From then on, various types of holograms have sprung up due to their remarkable exploits in optical applications such as data storage, 3D artworks, security, size checking, interferometric microscopy, holographic sensor[8-13].

Typically, a hologram can be recorded by projecting interference pattern on recording medium, in which the light scattered off objects (object beam) interferes with coherent beam (reference beam). The whole process is explained in terms of interference and diffraction, The whole process for holographic recording can be depicted in Figure 2.1.

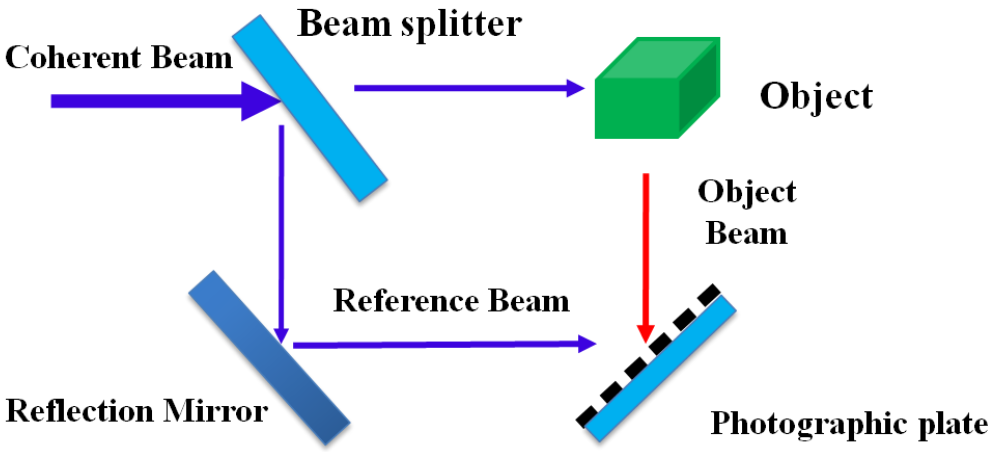

Figure 2.1 Illustration of holographic recording process

The image of object can be virtually reproduced by shining a laser beam, which is identical to the one used for recording hologram, to activate original light wavefront by means of diffraction [14]. It is somewhat like encoding of sound wave produced by a musical instrument, and later reproduces in a way without presence of original vibrating source, the simplified reconstruction process of original object wavefront is described as Figure 2.2:

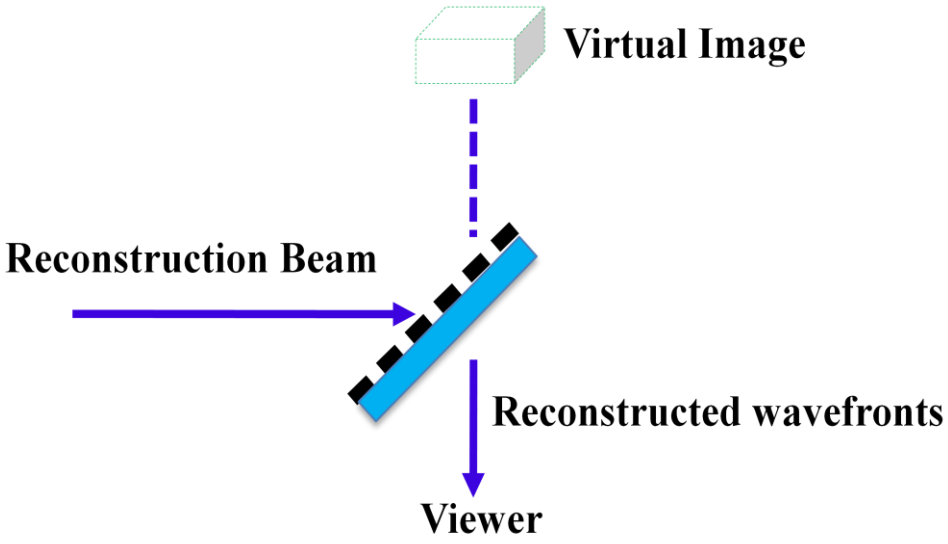

Figure 2.2 Reconstruction process for original light field

Obviously, in order to enable the record of a hologram, a laser beam is

essentially required to provide coherent beams. Specifically, a beam splitter should be applied to divide source beam into different beams, with each propagating in different directions. The beam which hits the scene interferes with the beam spreading through lens. In addition, the recording medium plays a significant role in the whole process. Several materials can be selected as photographic medium. In the early years, silver halide emulsions were among the most common materials due to their high resolution and sensitivity to light beam and the fact that it is easily available commercially. The following image (Figure 2.3) is an example of silver halide based-hologram

Figure 2.3 Silver halide based reflection hologram [15].

A diffraction grating is an example of holographic device. It can be fabricated by superposition of two plane waves from the light source on the holographic recording media. The interference of two plane waves result in straight lines across the recording surface corresponding to the varying interference intensity. When the grating is illuminated with only one beam which was used to create it. It can show

another diffracted wave appearing at the same angle as that at which the second wave was originally incident. In this way, the original object wave has been 'constructed'. Thus, the diffraction pattern is a holographic device as depicted in Figure 2.1 and Figure 2.2.

The principle of holography can also be characterised in mathematical model. An incident beam with single frequency can be modeled as a complex number **U,** the amplitude and phase of light are represented by absolute value and angle of the complex number. The objective and reference waves at any point are denoted as U_o and U_R, the magnitude of the combined waves can be expressed as :

$$|U_o + U_R|^2 = U_o U_R^* + |U_R|^2 + |U_o|^2 + U_o^* U_R \quad (2\text{-}1)$$

If a photosensitive recording medium is exposed to two beams, and its transmittance ,T, is proportional to the light energy hitting on the recording plate and is given by

$$T = kU_o U_R^* + k|U_R|^2 + k|U_o|^2 + kU_o^* U_R \quad (2\text{-}2)$$

where k is a constant. When the recording plate is illuminated by the reference beam, the light transmitted through the plate, U_H is equal to the transmittance T multiplied by the reference beam amplitude U_R, given

$$U_H = TU_R = kU_o |U_R|^2 + k|U_R|^2 U_R + k|U_o|^2 U_R + kU_o^* U_R^2 \quad (2\text{-}3)$$

Obviously, U_H has four items representing a light beam emerging from the hologram. The first item refers to the reconstructed object beam whose intensity is proportional to U_o, the second and third beams are modified versions of the reference beam. The fourth term is known as "conjugate objective beam". It has reverse curvature to the

object beam and forms a real image of the object in the space beyond the holographic plate.

2.2 Classifications of Hologram

There are various types of holograms since the first optical one was created in 1962. Actually, a hologram should contain one or more complex properties. For example, a transmissive hologram can also be amplitude modulated. Basically, holograms are classified into three different types due to different attributes, they are namely thin and volume holograms, transmission and reflection holograms, amplitude and phase modulation holograms.

As for thin hologram, it is defined that the thickness of recording medium is far less compared to the periodicity of interference fringes, and thus the thickness of recording medium can be negligible. In terms of thin (or surface) hologram, some research has been carried out to achieve certain applications. Professor Michal from Warsaw University of Technology [16] designed a thin multi-plane algorithm to enable the reconstruction of a colour hologram at different distances from hologram plane, the finest image (size and position exactly matches) could be reconstructed at a fixed distance under computational calculation and optimization. The following images (Figure 2.4) were recreated under the distance of 10 cm with equal average intensity and size.

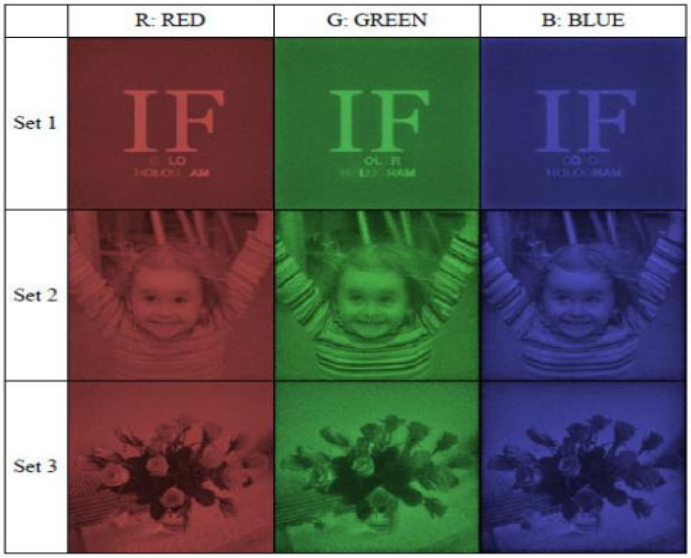

Figure 2.4 Numerical reconstruction of the hologram using wavelengths of a red, green and blue light at the distance of 10 cm [16]

Different from thin hologram which exhibit 2D features in photographic reconstruction, volume (or thick) holograms act as a selective colour filter which can only enable radiation with certain wavelength to be diffracted, the coating of recording medium should be much thicker than the spacing produced by coherent beams. In this case, the interference structure recorded in the recording medium is three-dimensional (3D), and it is shown that the incident light can only be diffracted at a particular angle which is known as Bragg angle [17]. However, if the incident angle for a light beam differs from the original reference beam, the reconstruction of original light field will take place at another wavelength and thus the colour of original object changes.

Due to its unique property of volume hologram, intensive research and study have been focused on this kind of hologram. In the year of 1997, a research group from Seoul National University successfully used speckle patterns of optical fiber to

behave as reference beam to write photorefractive volume hologram and produced hologram showed good spatial selectivity for spatial multiplexing [18].Hanhong Gao with his colleges designed a volume hologram as a displacement filter to selectively minimize the background noise in the daytime of artificial satellites in 2013 [19], the diffraction efficiency plot was related with longitude distance away from daylight. The schematic is illustrated in Figure 2.5 :

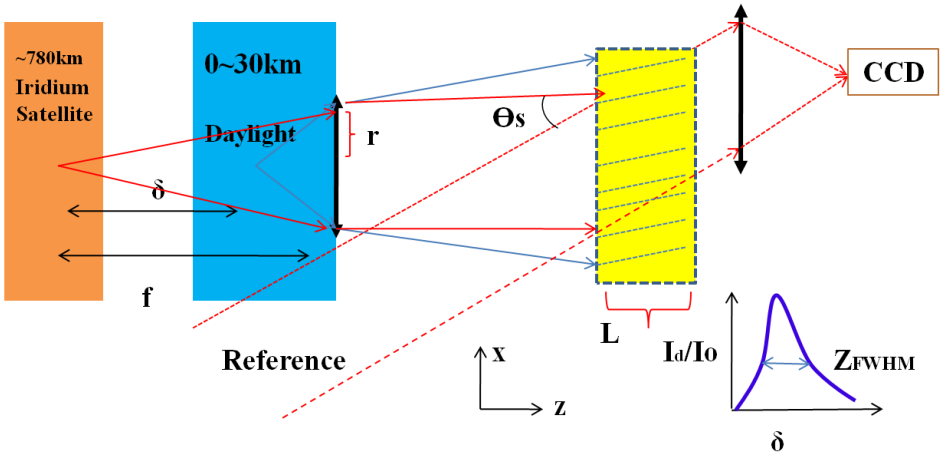

Figure 2.5 Volume hologram filter design set up [19].

Other than its application in sensing technology, volume holograms also show great potential in medical science. Professor Raymond K. from University of Arizona designed a degenerate volume hologram with broadband illumination [20]. it could provide low cost and high quality imaging and functioned as subsurface endoscope. Figure 2.6 was an example of ovary taken by degenerate hologram system under high NA microscope objectives.

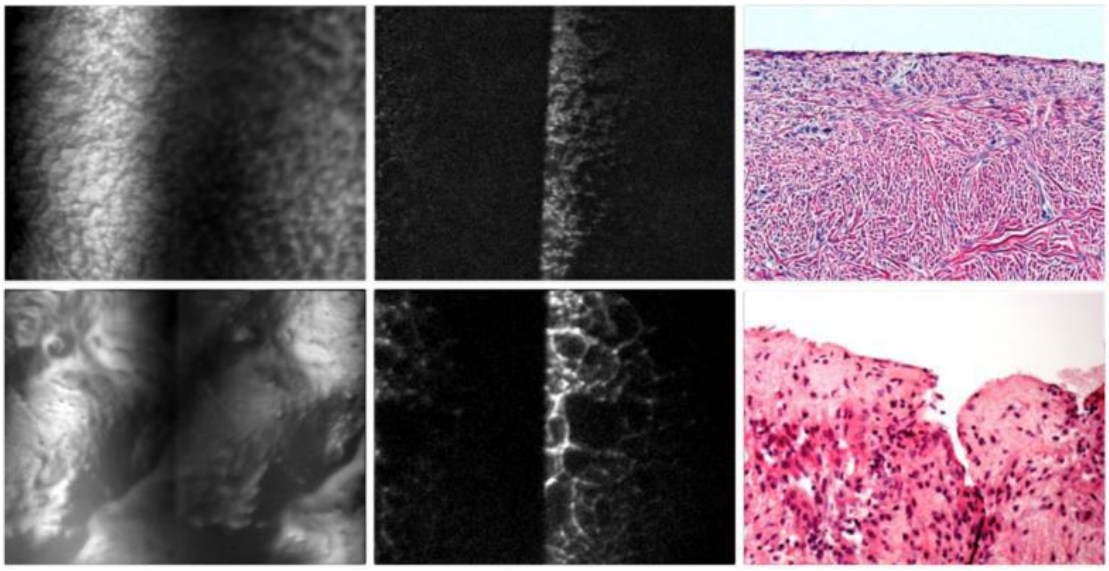

Figure 2.6 High quality images of normal ovary (top row) and diseased ovary (lower row) [20].

As for transmission and reflection holograms, they are distinguished by relative incident position from the recording medium. If the object beam and reference beam are incident on the plate from the same side, then a transmissive hologram is recorded. Otherwise, a reflective hologram is fabricated when the object beam and reference beam travel at opposite sides from the recording plane [21]. Usually, only volume hologram can act as reflective holograms because the diffraction efficiency is too low with thin film hologram. Early in 1984, high diffraction efficiency reflection-hologram was processed with silver-halide emulsion as recording material by Professor D.J. Cooke [22], the research aimed at improving the high-efficiency phase reflection holograms instead of transmissive ones. Nearly 75% diffraction efficiency (reflections was considered) of designed holograms could be achieved with the advantage of tanning developer acting on Agfa 8E56HD emulsion. Further to his research, Keiji and his team from Japan fabricated holographic polymer liquid crystal

and the efficiency was related to the size and density of droplet [23], it was seen that the reflection efficiency could reach the maximum of 70% when the size of LC droplet was nearly 0.2 μm and the density was 2E13 per cm^{-3}. The clear relationship between the reflection efficiency and features of HPDLC are given in Figure 2.7. It is apparent from Figure 2.6 that the reflective efficiency increased linearly with the decrease of droplet size and increase of density. It is manifested that the fabrication of phase separation structure could achieve high reflection efficiency.

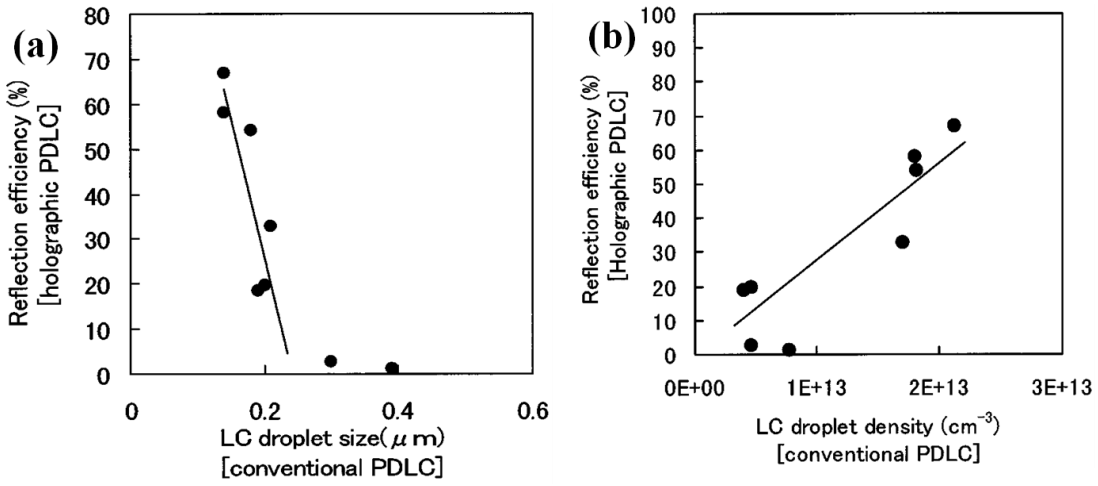

Figure 2.7 Relationship between reflection efficiency and LC droplet features. (a) Correlation between drop size and reflection efficiency. (b) Dependence of reflectivity on droplet density [23].

Additionally, some progress has been made in biomedical sensors regarding reflection sensors. In 2011, Domschke *et al.* [24] invented a method of making biocompatible sensor, consisting of a reflection hologram, which was able to detect the change of target fluid in body. This invention was specially intended for monitoring of glucose levels in ocular fluid of diabetics. In addition, the patent provided an inexpensive and cost-effective way for massive, large-scale production of

biocompatible sensors. It is quite significant because it can advance the technology in medical sensing domain.

When it comes to modulated holograms, there are mainly two types involved: Amplitude modulation hologram and phase modulation hologram. For amplitude modulation hologram, the amplitude of diffracted light is positively correlated with the intensity of original recording light while the phase modulated hologram is made by changing the thickness or refractive index of the recording medium in proportion to the intensity of interference pattern. Conventionally, a hologram contains two or more multiple characteristics. In this case, a volume-phase hologram is usually integrated and designed to enhance the diffraction efficiency to the maximum. Taken volume holographic grating as an example, it has exceptional properties such as compact, high-quality performance of imaging which cannot be achieved by traditional diffraction gratings. In addition, conventional diffraction grating are more vulnerable to surrounding environment, a slight physical contact may cause scrap and affect the diffraction efficiency. However, the volume phase hologram (VPH) is patterned physically which can survive in demanding circumstance. the structure of a typical volume phase grating is shown in Figure 2.8.

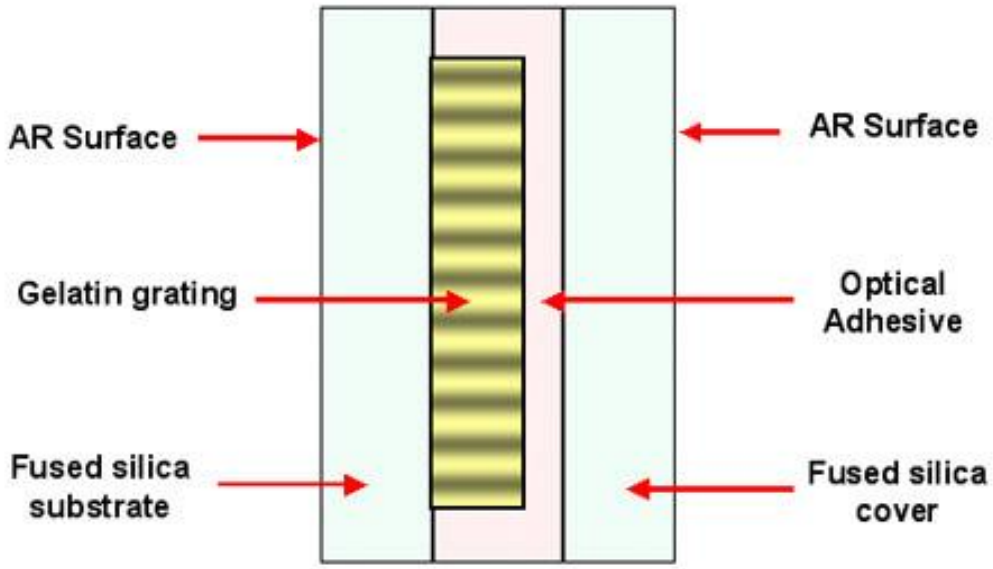

Figure 2.8 A volume phase grating hologram structure for transmission [25]

In addition, volume phase gratings show great potential in astronomical application, as they can be easily fabricated and customised to shape the grating, and they can be substitute for astronomical spectrographs for the versatile properties such as higher diffraction efficiency, higher dispersion, flexible configuration compared to surface-relief gratings.

With regard to ampitude hologram, it is substantially absorption hologram in which the transmittance lies on the exposure of recorded light. C.T. Chang in 1977 investigated the diffraction efficiency for amplitude holograms of both thin and thick types [26]. The thickness of hologram was modulated from 0 to 1, and for a certain modulated depth, thick reflection hologram contributed to highest diffraction efficiency, followed by the thin transmission and thick transmission hologram. The reason is that large amount of light passed through only a small fraction of recording layer, and thus the diffracted light for reflection remained the majortity. Overall, there are six types of holograms which are defined by different properties, they can be

applied separately under various conditions,as shown in Figure 2.9.

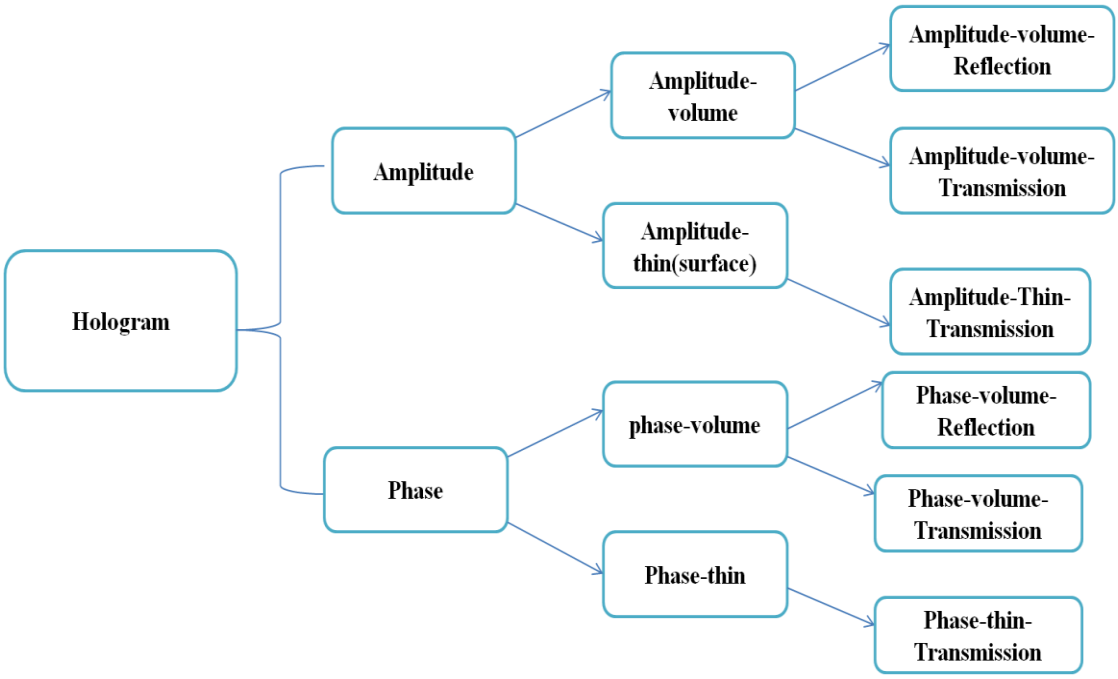

Figure 2.9 Diagram classification of hologram

2.3 Recording Medium for Holograms

To record a hologram, some necessary items are required, such as a suitable laser beam, collimator, beam splitter, and a stable environment which enables the thermal and other physical processes to proceed steadily when the interference pattern is being recorded [21]. However, in order to convert the interference pattern into an optical device, a specialised photosensitive material should be applied to record the optical information, namely recording medium.

2.3.1 Silver Halide Based Holograms

A diversity of holographic recording materials have been discovered and applied

to holographic recording, such as photographic emulsion, photorefractives, photopolymers, photoresist, photographic film and inorganic crystal [27]. In the early stage, the silver halide emulsion is the first material used for its advantages such as high sensitivity and cost-effective. It is the grains of silver halide crystal that is sensitive to light. Usually, the emulsion of gelatin goes through a complicated photochemical process, including light exposure, developing, fixing and bleaching. The whole process is illustrated in Figure 2.10.

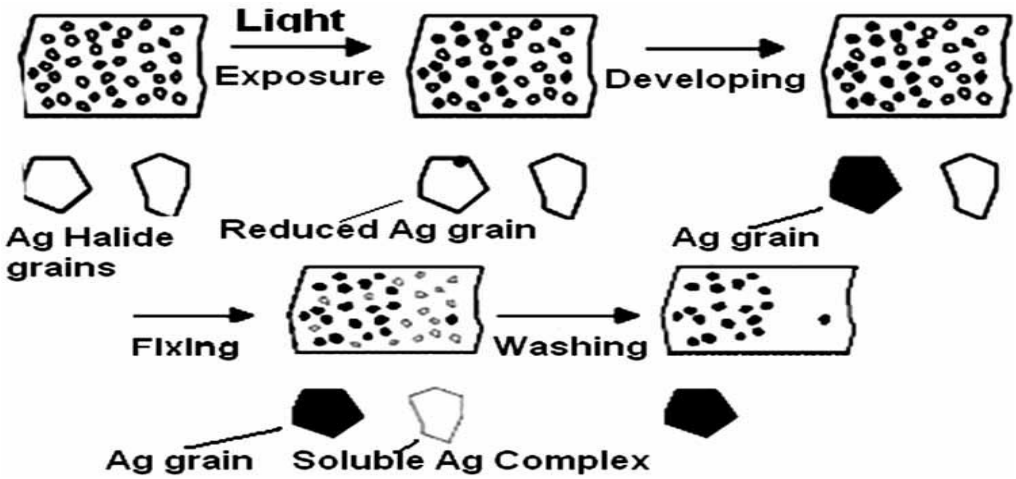

Figure 2.10 Process of silver halide for recording hologram [27].

Silver compounds are sensitive to certain part (up to 520 nm) of spectral bandwidth, in order to increase the sensitivity for other parts of spectrum, some sensitizers (dyes) are doped in the emulsion to broaden the sensitivity for spectrum. However, many kinds of dyes have their limitations when used as sensitizers. They have a relatively low solubility in water, and as a result, they are precipitated in presence of emulsion and cannot be adequately removed. The residuals of dyes are left in emulsion and in turn affect the recording performance of silver halide grains.

To improve the photoreaction efficiency and the quality of emulsion layer, an

invention was created in 1992 by adding trinuclear merocyanine into silver halide emulsion [28], the compounds were designed for sensitivity of spectrum ranging from 600 to 690 nm in red regime. The dye sufficiently dissolved in water and was rinsed away to a large extent after development and fixing of silver halide emulsion.

Processing for photographic substrate is also important after the selection of recording medium. When the silver halide is exposed to intensive radiation, it can be decomposed into metal silver which darken the plate. In order to weaken the effect of darkness, some work has been carried out, hardened dichromated gelatin has been used after exposure to light beam [29,30], Kim *et al.* invented a post-exposure method to improve the performance of emulsion layer, the silver halide layer was pre-harden after exposure and then developed in a developer. Subsequently, the layer was bleached and hardened twice. After trying, it went through surface-hardening and fixing. Finally, the processed layer was rinsed in warm water and dried again for finish. The post-exposure process improved largely the sensitivity to light and increased the colour reproducibility, and energy sensitivity.

The resolution of silver halide emulsion is dependent on many factors, such as light illumination, grain size of silver halide crystals. The defect and insufficiency in silver halide grains can directly affect the quality of reconstructed image [27]. As a result, refining the grains of silver halide is of great importance to enhance the diffraction efficiency. Up to now, diverse methods have been used to obtain fine grain silver emulsion. In one invention, Shigeharu *et al.* used a mixed aqueous solution by

water-soluble silver and water-soluble halide [31], to prevent the sliver from growing bigger by expelling the formed grains out of the mixing vessel, the size of produced silver grains was controlled to be ~0.05 μm.

Another technology called silver halide sensitive gelatin (SHSG) is introduced for making holograms [32]. This technology incorporates the high sensitivity of silver halide emulsions with the superiority of high diffraction efficiency and low scattering effect from dichromated gelatin.

Generally, the SHCG technique undergoes the exposure and tanning process. After fixing, the silver salt or sliver will spread out and result in transparent pure gelatin. Finally, the left gelatin is dehydrogenated by using a hydrophilic organic solvent, the gelatin has a refractive index of 1.5, and the refractive index of air throughout the voids is 1.0. The difference between the refractive index yield high diffraction efficiency up to 96% [32].

2.3.2 Photopolymer Based Hologram

Silver halide materials are proved to be quite suitable for making holograms and hologram replication. However, the drawbacks and disadvantages are attributed to large absorption of incident light, inherent noise, and tedious processing which are quite time-consuming and labour-intensive [27]. As for photoresist or dichromated gelatin, they are less expensive and require less process. Nevertheless, these materials still go through wet processing steps to develop and fix the image, which causes the

delay of availability.

In regards to photopolymer, it is a kind of material which changes its property when exposed to light, mainly within the regime of visible spectrum or ultraviolet [33]. The free radicals are produced when the photopolymer is illuminated with incident beam, the radicals then react with monomer molecules and result in vinyl polymerisation in exposed area. The polymerization process reduces the chemical potential of monomers in bright region. Consequently, the monomers in dark domain merge into the bright regions. It is manifested to be structurally changed called curing, Figure 2.11 is an example showing the cross-linking and hardening effect of polymerization when exposed to light.

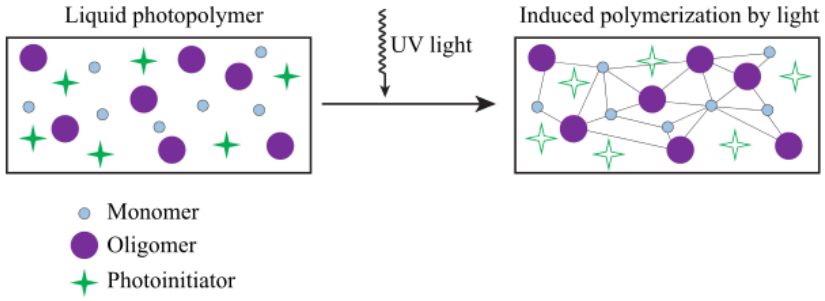

Figure 2.11 Illustration of curing process [34].

The changes of chemical and structural properties for photopolymer can be accomplished by internal stimulation of chromophores which polymer subunit already have or externally activated by photosensitive materials. Usually, a photopolymer is comprised of monomers and oligomers to fulfil certain physical properties. In some cases, photo-initiators are needed to activate the process of curing as some polymer systems are not readily activated by light. An example of cross-linking process is

shown in Figure 2.12 by the mixture of monomeric styrene and oligomeric acrylates [34].

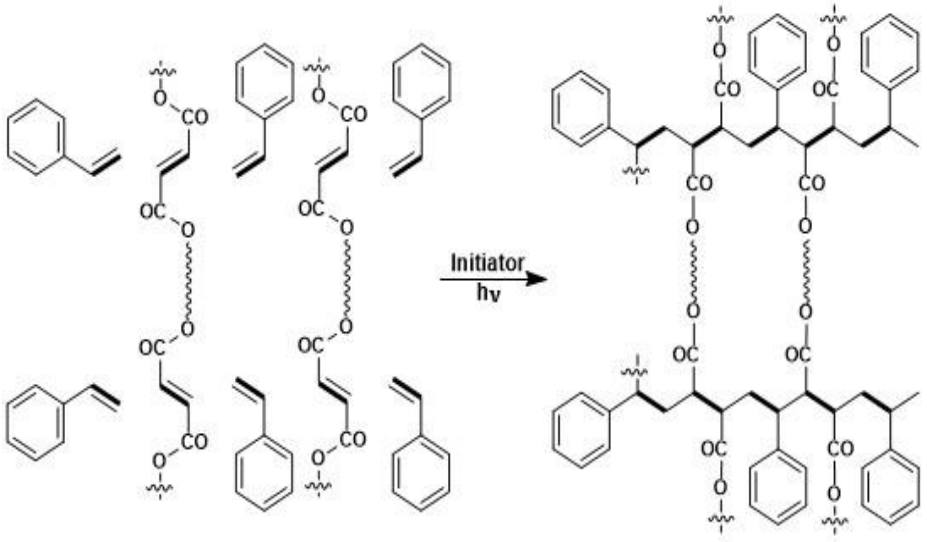

Figure 2.12 Cross-linked polymer structures through polymerization by Monomeric styrene and oligomeric acrylates [34].

Understanding the photochemical mechanisms is quite significant to the process of recording a hologram. When recording a hologram, the polymerization only can be initiated at the region where the coherent beams complete the constructive interference while no polymerization occurs at destructive interfering zones, the scheme of holographic recording process based on photopolymer material is depicted in Figure 2.13:

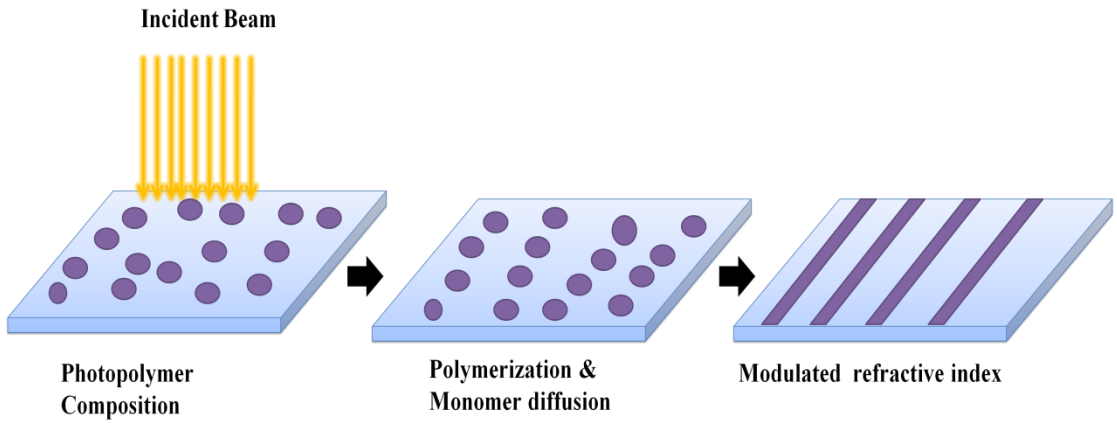

Figure 2.13 Holographic recording on photopolymer film

A lot of research and reports have been done on photopolymer based holograms, the first invention of photopolymer based hologram can be traced back to 1970s when inventor Haugh created a permanent image made by photo-polymerizable materials, the image produced had high resolution and stable to exposed actinic light. It was just single-step process and diffraction gratings as well as copies of holograms can be easily made corresponding to the invention [35]. Ever since a vast number of applications based on photopolymers have been exploited. The great advantage for photopolymer induced hologram is that it only undergoes a single step instead of a series of complicated wet processes as silver halide does. This helps to reduce the cost of recording hologram and enables the massive and rapid use in industry. It is also found that the photopolymerizable material can ensure high sensitivity as well as excellent storage stability [27].

In 1990, fluorinated binders incorporated in photopolymer compositions were compounded to produce excellent reflection hologram [36], the modulation value for refractive index was higher than 0.01. Therefore, the compositions are especially

suitable for applications where high reflection efficiency is required, such as holographic optical elements, notch filter, or others like that. The diagram of recording the reflection hologram on photopolymerizable layer is shown as Figure 2.14.

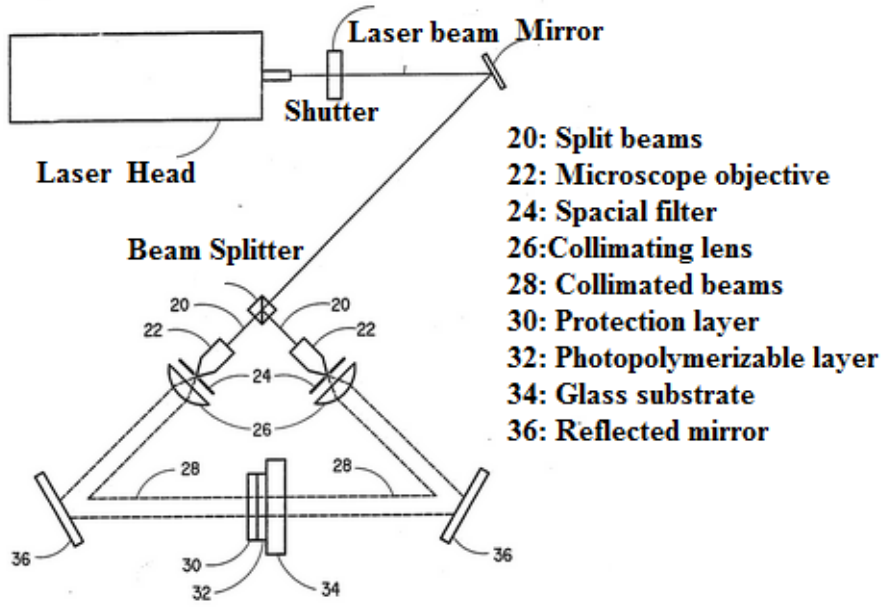

Figure 2.14 Configuration of holographic recording system for photopolymerizable material [36].

Holographic sensors including photopolymer-based holograms are also invented. Naydenova *et al.* [37] explored the response characteristics to humidity and temperature of volume phase grating recorded in photopolymers. The photopolymers were comprised of acrylamide and diacetone as monomers and triethanolamine, N-phenylglycine as photoinitiators. It was found that the in the range of RH = 20%-90%, the humidity sensitivity is strongly dependent on the diacetone acrylamide-based transmission grating's diffraction efficiency, the temperature response of slanted transmission grating were also investigated under the range of 20

to 60 ℃, the Bragg angle for diffracted light shifted due to the shrinkage effect of photopolymer layer by water evaporation. The fabrication approach of photopolymer-based holographic gratings can be applied to produce holograms tunable with temperature and humidity which can be of great use for practical sensing domain.

Furthermore, the photopolymer-based holograms can be also applied to security and optical data storage. In 1994, Jean J employed micro holograms into very small parts of a card [38], the recording area was about 10 to 100 microns, the free radical ethylene monomer was initiated by the combination of polyethyleneimine and lithium acrylate. The aim of producing micro holograms on card was to prevent forgery cards to access in. The altered card can produce different diffraction image compared to that of an original real card. Researchers from Taiwan developed a circular polarized volume hologram in photopolymer [39], the components in photopolymer materials were PMMA monomer and photosensitive phenanthrenequinone-doped molecules. Based on a series of experiments and theoretical analysis, a circularly polarization recording configuration was set up to create polarisation multiplexing holographic memory to store optical data. Moreover, Researchers from Dublin Institute of Technology designed holographic optical elements to collect light energy from a moving source [40], a combination of gratings were incorporated into a holographic solar collect to allow for a broad range of incident angles. The optimum diffraction efficiency for recorded holograms were over 80% and the optimal intensity for recording holograms were found to be 1 mw/cm^2 at a spatial frequency of 200 l/mm.

In this work, the relationship between the thickness of recording medium, spatial frequency and angular selectivity was discussed, the following image demonstrated the photopolymer focusing elements recorded, the photopolymer was sandwiched between two protective layers. The light-collection device contained arrays of multiple diffraction grating elements.

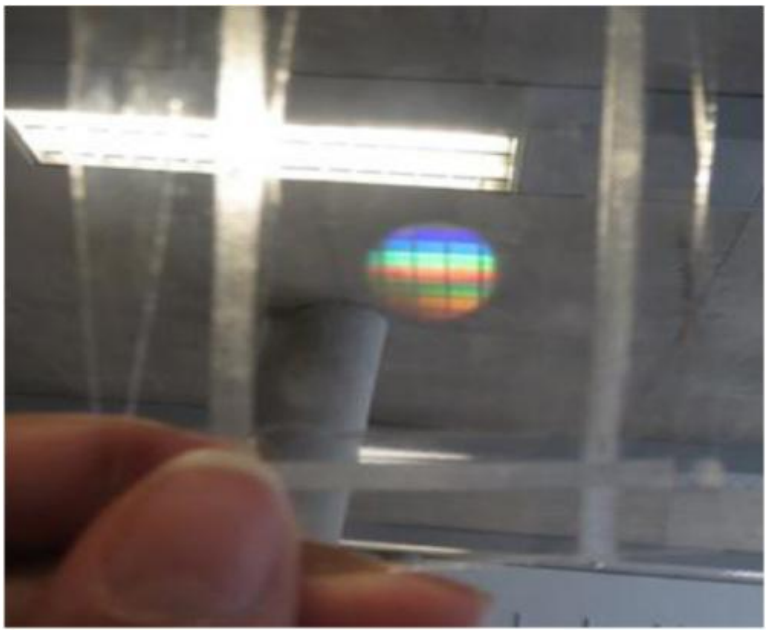

Figure 2.15 Optical holographic elements recorded in acrylamide photopolymer [40].

2.3.3 Photorefractive Material

The photorefractive effect is seen in certain crystals and other materials which can alter their refractive index when illuminated with light beams, it is typically a non-linear effect [41]. For photorefractive materials, they have broad use as they are ideal medium for erasable and dynamic holograms. They can also be used as optical data storage device temporarily [42].

The photorefractive reaction usually undergoes some certain stages. The target

material is primarily illuminated by coherent beams (object and reference beams), and interference pattern is recorded in the medium where black and white fringes are formed. Within the bright region, electrons can absorb the energy of light and be stimulated from impurity level to the conduction band of the material, leaving an electron hole with positive charge. The electrons are totally free when they are in conduction band, they can move or diffuse throughout the material. As the electrons are excited originally from bright region, they will shift to dark area and result in diffusion current. By the redistribution effect of electrons in the photorefractive materials, the resulting current forms an electric field, defined as spatial charge field. The electric field can still exist when the light is removed cause the electrons and holes are trapped and stay unchanged. Furthermore, the formed electric field, together with photoelectric effect, lead to the change of refractive index throughout the crystal according to the varied intensity, and the pattern recorded is identical to the interference of coherent beams [43].

Applications have been carried out for its unique properties of photorefractive materials, especially in the fabrication of dynamic and erasable hologram. In the year of 2000, Arosha *et al.* from Stanford University applied the photorefractive-based hologram to the image amplification and novelty filtering [44]. They wrote a volume hologram in a photorefractive composition, and 37 times amplification of image intensity was observed within one frame time (~33 ms).

Photorefractive-based holograms also have great potential in data storage and reading. In one invention, holographic stereographic technique was utilized to write a

refreshable image at frequency of two seconds based on the medium of photorefractive polymer [45]. The multiplex holographic recording system was also demonstrated in order to shorten the recording time for full parallax, as shown in Figure 2.16, the holographic optical device (HOE) is used to modify the transmission direction to intersect with object beams onto the surface of photorefractive layer.

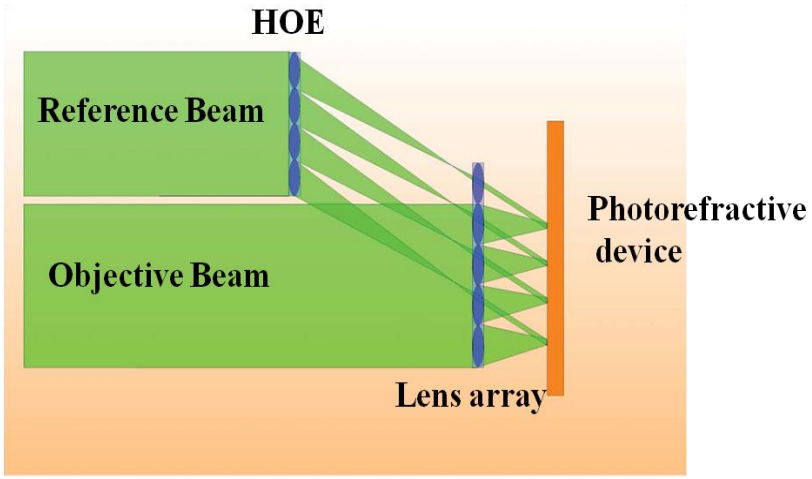

Figure 2.16 Sketch of full parallax recording [45].

By using the multiple recording system, simultaneous recording of 100 hogels (pixels which contain 3D information from various perspectives) were able to be recorded by a 6-ns single laser pulse. The images shown in Figure 2.17 were viewed from two different perspectives by full parallax holographic recording system.

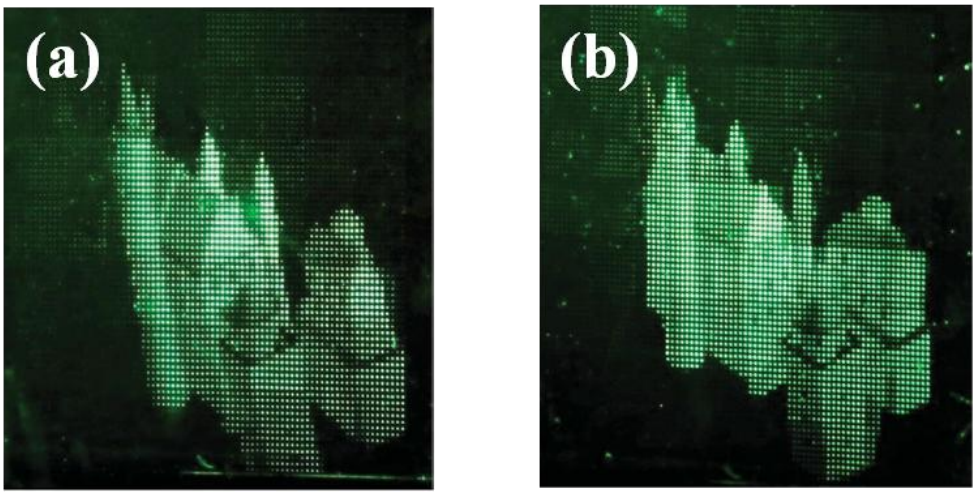

Figure 2.17 Example of full parallax hologram representing castle and towers. (a) From up-right perspective. (b) From up-left perspective [45].

In addition to the dynamic and real-time refreshable holograms, they also developed a telepresence system with which the image produced can have face-to-face effect even the actual distance is far away. This technology is especially significant when applied to remote control or detection. For example when a surgical operation is conducted, through which the surgeons are able to monitor the real time 3D images and get involved in practical procedures.

2.3.4 Other photographic recording medium

Other than the materials mentioned above, there are an abundance of advanced materials which are applied for holographic recording. Each individual material possesses its advantages and drawbacks. For example, silver halide based hologram has high diffraction efficiency, but the photochemical process for silver halide is costly and labour-intensive. As for photopolymer, it is relatively fast and can have polymerization effect when exposed to light, which avoids the complicated wet processing. However, it can cause possible distortions due to shrinkage during polymerization process, which limits the spatial resolution of hologram.

Inorganic nanoparticle doped photopolymers were reported by Suzuki *et. al.* and Tomita *et. al* [46-47]. The inorganic nanoparticles are chosen for the reason that they have a wide variety of refractive index, which offers larger index change throughout the photopolymer layer. The included nanoparticles can also suppress the possible

shrinkage during polymerization process.

A recent invention used polyelectrolyte to be holographic recording medium and achieved high diffraction efficiency. It was selected for its advantages such as non-toxicity, water solubility, high productivity and less expensive as compared to silver halide material. Figure 2.18 illustrates the typical structural units of polyelectrolyte.

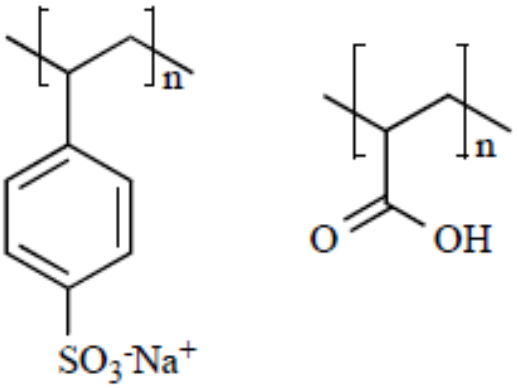

Figure 2.18 Structural units of typical polyelectrolyte [48].

Overall, there are plenty of recording media to be utilized for holographic recording, they all play significant roles throughout the whole recording process because the interference pattern is directly recorded into the medium and later be replayed from the holographic medium corresponding to original light field. Consequently, the diffraction efficiency and quality of images largely depend on the performance of recording medium, and various attempts are made to increase the diffraction efficiency, decrease the polymerization related shrinkage, minimize the post processing. Regarding future development for holographic recording, the properties of ideal recording material should progress towards higher resolution, less

expensive, simpler process and less labour input. A histogram presenting the hologram patents made by a variety of materials are shown in Figure 2.19.

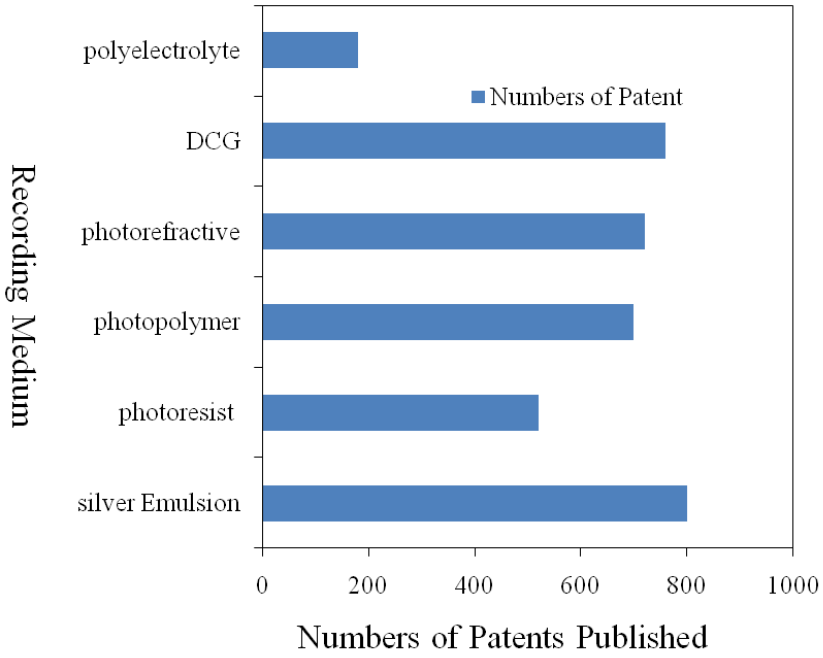

Figure 2.19 Holographic patents published based on a variety of recording medium [27].

2.4 Holographic Fabrication Methodology

Traditionally, a hologram can be constructed by coherent beam interference wherein a beam splitter is necessary to split beam source to multiple beams. In this situation, the laser system is required to provide precise alignment and sufficient stability to enable stable interference of object beam and reference beam. Many fabrication methods have been proposed and carried out ever since the first optical hologram made in 1960s [1]. Surface stamping or imprinting is a common technique for making surface holograms by means of embossing [49-51], and many holographic applications have been successfully carried out through this method. For example, the

hot stamping technique has been a proven technique which is applied extensively in manufacture industry. It is a dry printing method of lithography in which pre-dried ink or foils are transferred to a substrate at high temperatures. One application of hot stamping hologram is to attach a range of holographic foils to the surface of package to add extra visual appeal and attract more attention from customers. The most famous application case for holographic hot stamping is security identification. The following images (see Figure 2.20) are examples of security holograms made by surface stamping.

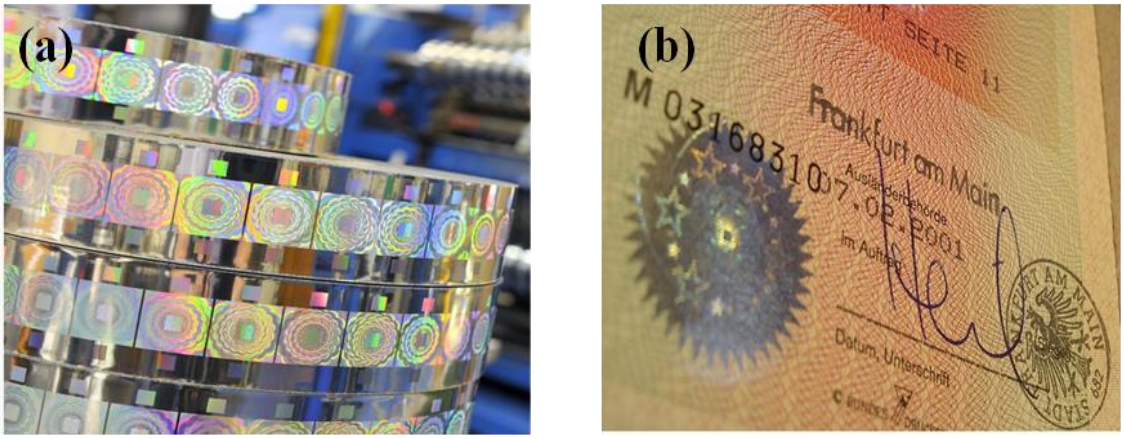

Figure 2.20 Examples of security holograms by embossing. (a) Production of hot stamp security foils. (b) Identification of residency permit [51].

More complex fabrication approaches, including E-beam lithography (EBL) and focused ion beam, are also utilized to implement the fabrication of holograms. In 2012. Butt *et al.* developed a CNT (carbon nano tubes) array hologram which was fabricated using a nano beam electron beam lithography system [52]. The patterned CNT arrays exhibited a high resolution diffraction image of "Cambridge" with the illumination of red, green and blue lasers. The proposed method is quite significant as it paves the way towards the utilization of nanostructures in 3D hologram fabrication

and its application to a broad range of nano optical devices. In another invention, Montelongo *et al.* from University of Cambridge fabricated the nanoantennas on top of 200 nm silicon dioxide via electron beam lithography [53], the designed hologram was able to conduct polarisation switchable diffraction by controlling the orientation of electric field of a beam. Figure 2.21 demonstrates the polarized diffraction from simulation and experiment results by nanoantenna under different orientation of electric field. Nanoantennas only response to the electric field which is along its corresponding axis. Orientation of 45 ° for electric beam can result in diffraction for both of nanoantennas.

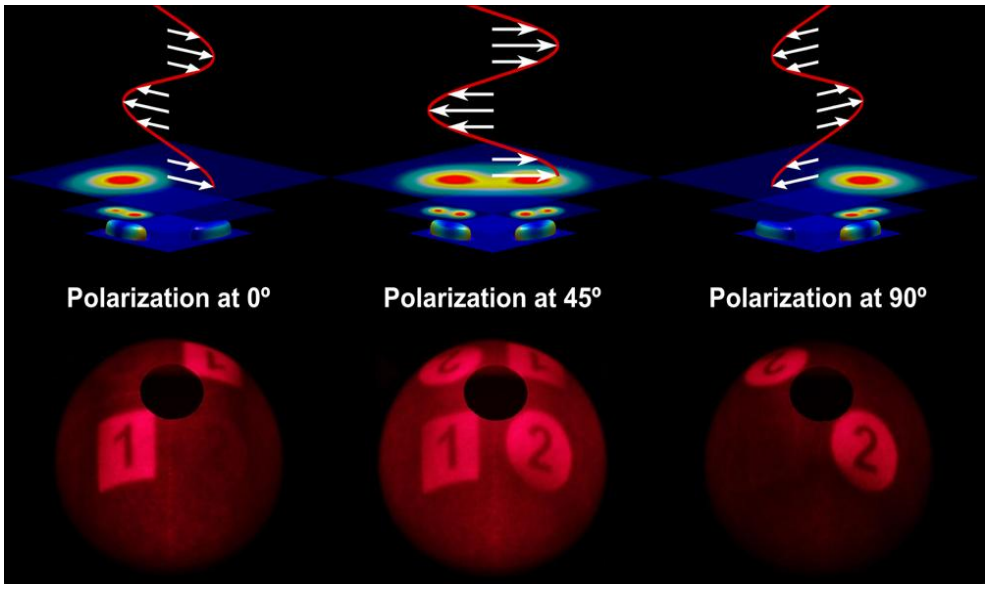

Figure 2.21 Simulation and experimental results for two polarised holograms [53].

For holograms which are fabricated by focused ion beam (FIB), it is a milling process normally completed within minutes or even hours. The fabrication of FIB is mainly used in electron holography. In 2005, David cooper [54] utilized low temperature annealing process to improve the electron holographic phase image of GaAs-Si by FIB milling, the noise was largely reduced in phase images recorded

using off-axis electron holography.

Although the EBL and FIB can achieve high resolution holograms and even be applied to nanoscale optical devices. However, the processing time of fabrication is relatively long (ranging from several hours to a couple of days depending on the ablated area and exposure time) and results in less throughput and high cost. In addition, the produced defects or artefacts may also affect the resolution and quality of prepared holograms.

To overcome the limitations mentioned above, direct laser interference patterning (DLIP) in split-beam off-axis mode has been utilized to ablate surface gratings. Laser pulses (Power intensity: 275-300 mJ/cm ^{2}) were utilized to ablate a series of materials including polymers, nickel, and steel [55-57]. This ablation setup can be integrated with an optical head with variable spatial period from 0.40 to 3.75 μm at a working distance of 35 mm. In another fabrication method, a frequency-quadrupled diode-pumped solid-state laser (6 ns, 266 nm, 20mJ) allowed direct interference ablation of light-emitting fluorene polymer ADS133YE to create gratings that were 5 mm in diameter [58]. Ti:sapphire laser with regenerative amplification (130 fs, 800 nm) was also utilized to created surface gratings in polymethyl methacrylate (PMMA) [59]. In these approaches, the incident laser beam has to be split into two or more beams to interfere with each other. The reflective mirrors and splitter must be aligned accurately to allow maximal interference. Furthermore, this kind of approaches limit the use of 3D images of objects due to significant lose of energy passing through the beam splitter. Hence, the ability to print 2D gratings and/or 3D images with the use of

a single laser pulse in an optically flexible mode remains a big challenge. Besides, inexpensive and appropriate materials, simple processes, quality of recorded holograms are necessary to be taken into consideration.

2.5 Conclusions

Overall, In order to enable practical making of holograms, multiple items are needed and have to cooperate with each other. A suitable laser source, a suitable object, a robust laser system which supports the stable interference of coherent beams, an appropriate recording medium to perform good resolution and high diffraction efficiency.

In this chapter, different kinds of holograms are classified and the characteristics and applications for each kind of hologram are demonstrated. As an important element, the optical recording medium ranging from silver halide emulsion to nanoparticle doped photopolymer, are discussed. Despite its high resolution (~5000 mm^{-1}) and easy availability for silver halide emulsion based holograms, they suffer from several problems such as high absorption characteristics, inherent noise, complicated wet processing, irreversible recording which turn out to be labour-intensive, time consuming and costly, limiting its further application for massive production. Meanwhile, photopolymers seem to be promising holographic recording media. However, the decrease of polymerization related shrinkage and distortion still remains challenging to ensure the high resolution (5000 mm^{-1}) of formed holograms. Regarding future holographic recording medium, it is expected

that materials with high sensitivity, less post processing, less shrinkage or distortion should be supported.

On the other hand, several holographic fabrication methodology are presented and described. For microfabrication methods like EBL or FIB based holograms, they can both offer high resolution (nanometer scale, ~2 nm) capability and well-ordered diffraction pattern. However, because of their limited throughout and intensive input of energy and complex systems, they are not suitable for high-volume manufacturing. In addition, multibeam interference techniques are introduced to pattern large-scale areas which are time-saving and efficient. However, the multibeam system requires complex and precise alignment and it has proven difficult to control the shape and position of interfering area, which imposes restrictions on 3D holographic patterning. Thus, the rapid, simple, cost-effective laser interference system with high throughput should be the main trend for future holographic fabrication.

After the complete literature review and knowledge base on holographic fabrication. A strategy of single laser pulse in optically flexible mode using low-cost material to achieve rapid production of 2D/3D customized hologram is proposed, which will be presented in the following chapters.

3.Holographic Ink-based Grating Fabrication

3.1 Introduction

In this chapter, a one-step, feasible and low-cost holographic recording technique is introduced, in which a nanosecond laser pulse is directed to project interference pattern on any surface coated by light-absorbing materials. The light used to record the hologram is only single laser beam instead of multiple beams. Printable ink was chosen to be recording medium. The printable ink was supplied from Staedtler (Germany) and it is a light-absorption material which is permanently coated on the substrate. Computational simulation was conducted to predict the spacing for ablated gratings. A series of optical images were also taken to characterise the formation of ablated grating holograms. Experiments of angle-resolved measurements were also conducted on surface grating sample to obtain the diffraction characteristics of grating holograms.

3.2 Holographic Recording Setup

The surface holograms were recorded according to “Denisyuk” reflection interference in ablation mode, the laser setup is shown in Figure 3.1. A Nd-yttrium-aluminum-garnet pulsed laser was generated and emitted (central wavelength: 532 nm) from a second-harmonic generator (5 ns, 350 mJ, 10 Hz, thermally stabilized with wavelength separation). The beam was directed by mirrors and travelled through a beam expander. Unlike the photochemical reaction, the laser

ablation is a physical process during which high peak power is able to remove and ablate the material which is defined by the threshold in certain site of coating layer, the shape and formation of ablated pattern depend on the comprehensive factors including laser pulse duration, localised energy of laser beam and absorption property for target material.

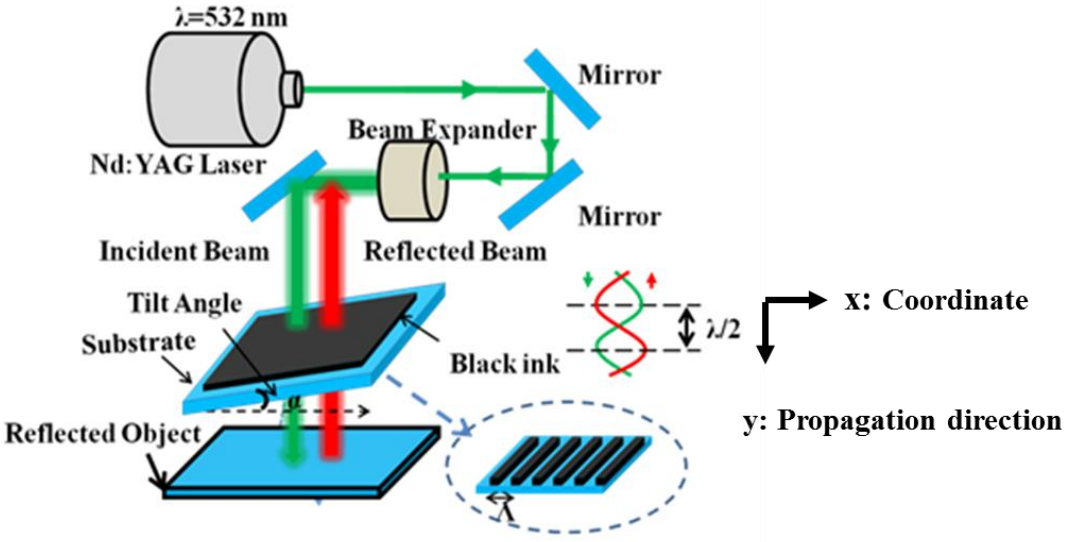

Figure 3.1 Schematic of single laser beam setup [60].

A 150 nm thick of ink (Lumocolor, Staedtler) was deposited on a PMMA substrate at a spin speed of 2100 rpm for 3 s prior to recording. The recording plate was tilted at an angle of α from the horizontal plane. In a single 5 ns exposure, the ablated spot area was about 1 cm^2, revealing that a grating over an area of 1 cm^2 required 5 ns. To ablate large scale of grating, multiple laser exposures were required to cover 5 cm^2 by manually moving a XY translation stage. Therefore, the use of robotic XY translation stages can increase the ablation area directly. Finally, a reflecting object (i.e. mirror or coin) was placed normal to the laser incidence beam under the recording medium, the incident laser beam illuminated on the flat reflecting

object and reflected off. The interference occurred when the incident beam and reflected beam travelled in the opposite direction. Creating a standing wave which showed a periodic constructive interference. The ink was then ablated at a periodicity according to the incident wavelength of the laser beam given by equation 3.1:

$$\begin{aligned} y = y_1 + y_2 &= A\cos 2\pi(vt - \frac{x}{\lambda}) + A\cos 2\pi(vt + \frac{x}{\lambda}) \\ &= \left|2A\cos 2\pi \frac{x}{\lambda}\right| \cos 2\pi vt \end{aligned} \tag{3.1}$$

where y_1 and y_2 represent the propagation equation for incident beam (object beam) and reference beam (reflected beam), respectively. *A* refers to the magnitude of the electrical field and *x* is the coordinate along the propagation direction. From the resultant equation, it is found that the standing wave oscillates in time, but has spatial dependence on the propagation direction which is stationary, the constructive interference occurs at half wavelength (λ/2) of incident beam. Since the recording substrate is tilted from horizontal, the periodicity of grating can be deduced as the following equation:

$$\Lambda = \frac{\lambda}{2\sin\alpha} \tag{3.2}$$

α is the tilt angle between the recording plane and horizontal plane, and λ is the wavelength of incident laser beam. In order to verify the theoretical equation, 2D intensity distribution by standing wave was simulated via finite different time domain method (FDTD). Figure 3.2 shows uniform intensity variation ranging from red (strongest) to green (weakest) by single beam interference with the wavelength of 532 nm, indicating well-ordered grating pattern.

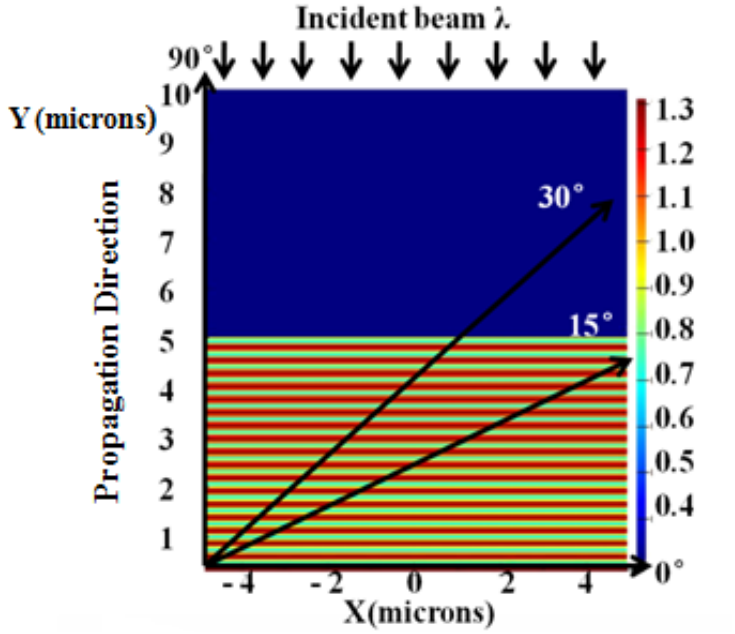

Figure 3.2 2D simulation of interference pattern by single beam interference [60].

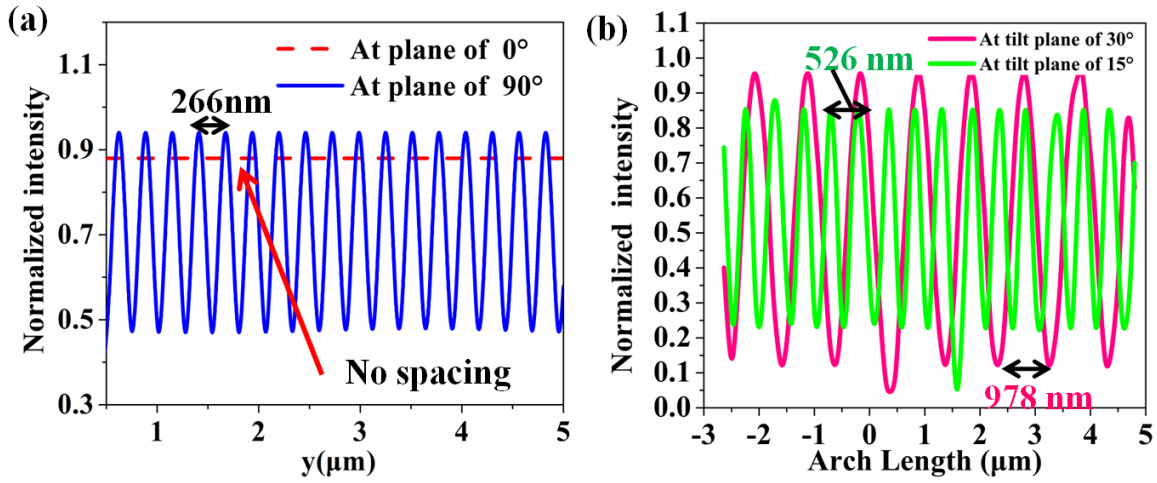

Figure 3.3 Intensity profiles across at multiple planes (a) 0 ° and 90 °. (b) 15 °and 30 ° [60].

The intensity profiles with regard to different tilted planes were plotted in Figure 3.3. There was uniform spacing of ~260 nm at the plane of 90 ° while no varying intensity was observed at horizontal plane (0 °), and thus no grating will be formed when the recording substrate is placed normal to propagation direction. The grating periodicity at planes of 15 °and 30 ° were simulated to be 978 nm and 526 nm,

respectively. From the calculation of equation (3-2), it is apparent that the simulated periodicity was in good agreement with the calculated values. Specifically, by changing the tilt angle of recording device, the spacing of gratings can be easily controlled and modulated. Microscope images were taken to observe the morphology of surface grating by a Zeiss Axio Scope under dark field, as shown in Figure 3.4(b).

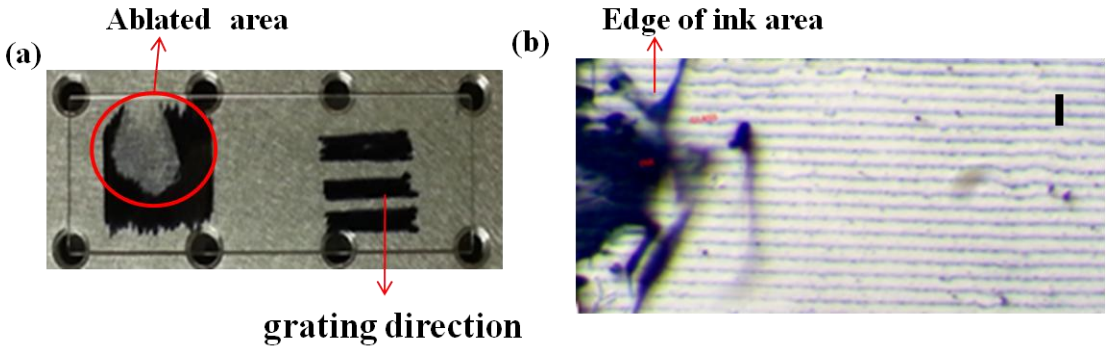

Figure 3.4 Images for prepared ink sample. (a) Camera image of the ink-based grating sample. (b) Microscopic image taken with magnification of 100x. Scale Bar = 5 μm.

It is obvious that the grating sample showed legible grating pattern on the surface. However, uneven ablation was observed with the center much better defined than regions around the outer edges. This may be attributed to the beam profile, beam energy and irradiation being more intensive in the center compared to edge areas. The microscope image showed clear evidence of evaporation process: the ink had "bubbled" unevenly off the surface to form various ink flecks. In addition, the outer edge of spot, where only some parts of the ink have evaporated, leaving a rough transition boundary, this indicated the region where the ink melted or vaporised, but didn't complete the whole process due to insufficient laser energy.

In order to obtain accurate topography and periodicity of holographic grating,

scanned electronic scanning microscope (ESEM) and atomic force microscope (AFM) were conducted, the images are shown in Figure 3.5.

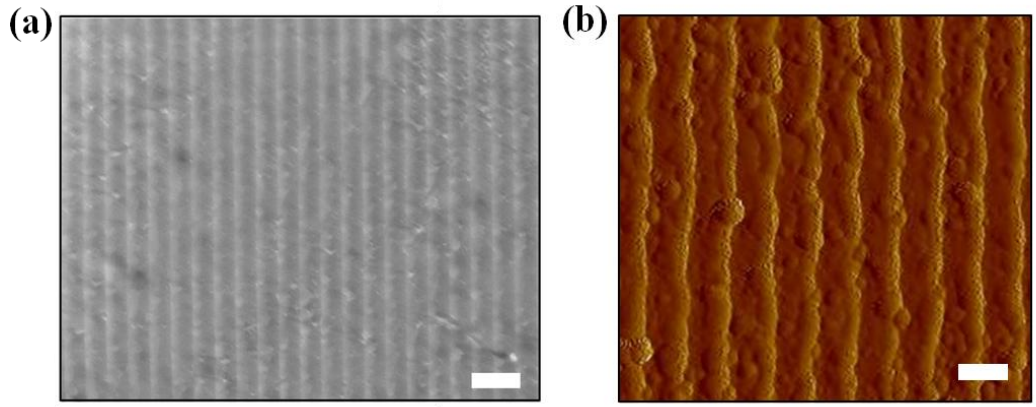

Figure 3.5 Images of recorded linear surface gratings. (a) SEM image of the surface ink grating. Scale bar = 5μm. (b) AFM characterization showing thickness and spacing of surface ink-grating. Scale bar = 3μm [60].

The SEM image showed a well-ordered grating with periodicity of ~2.6 μm, which is in good agreement with equation 3.2. Additionally, an average thickness of ink layer was measured to be ~150 nm by AFM characterization. Both images illustrated well-ordered grating pattern ablated by single laser beam interference with the tilt angle of 6 ° from the surface plane of the mirror.

3.3 Optical Simulation of Ink-Based Grating

Before detecting the optical diffraction characteristics by carrying out experiments, optical characteristics for ablated ink-based grating were simulated to predict the possible diffraction pattern. Finite element method (FEM) method by COMSOL Multiphysics were utilized to carry out the simulation, the optical simulation was conducted in the radio frequency model, a hemisphere boundary with a diameter of Φ32 mm was setup to monitor the diffraction pattern, the boundary condition was set to scattering boundary so that there was no reflection on the boundary when the plane wave is normally incident, the simulation was processed in the air environment with a relative permittivity of $\varepsilon_x = 1$. The silicon dioxide substrate has a relative permittivity of $\varepsilon_x = 4.2$ at room temperature, the refractive index of ink was set to be 1.6 based on the material parameter. Three different plane waves with wavelengths (405, 532, 632 nm) were induced to illuminate perpendicularly on the ink-based grating. The dimensions and shape of grating were constructed according to the morphology presented by ESEM and AFM images (spacing~2.6, arc-like grating) . The overall geometry for optical simulation is shown in Figure 3.6.

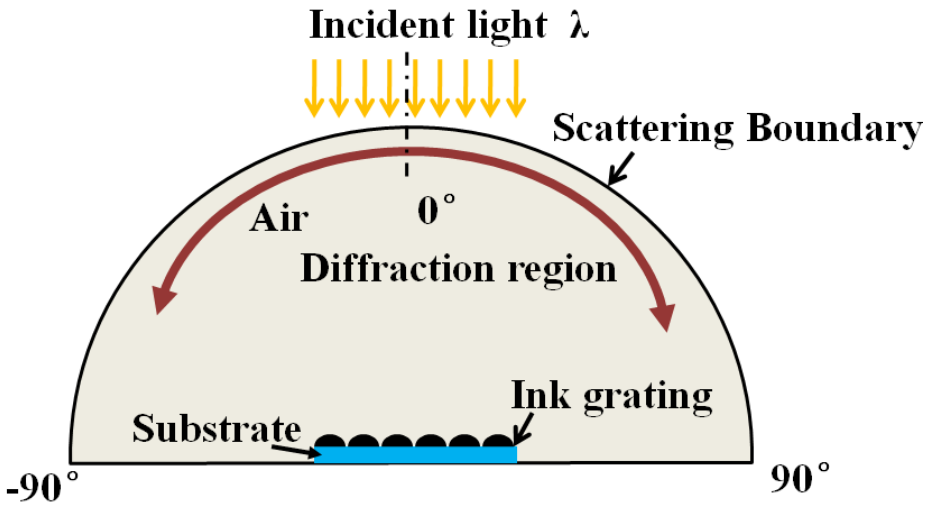

Figure 3.6 Illustration of 2D FEM simulation model by normal incidence [60].

The diffracted spots are shown symmetrically on the hemispherical boundary in response to red light (Fig. 3.7(a)), up to four diffraction orders were observed from each side of the incident beam.

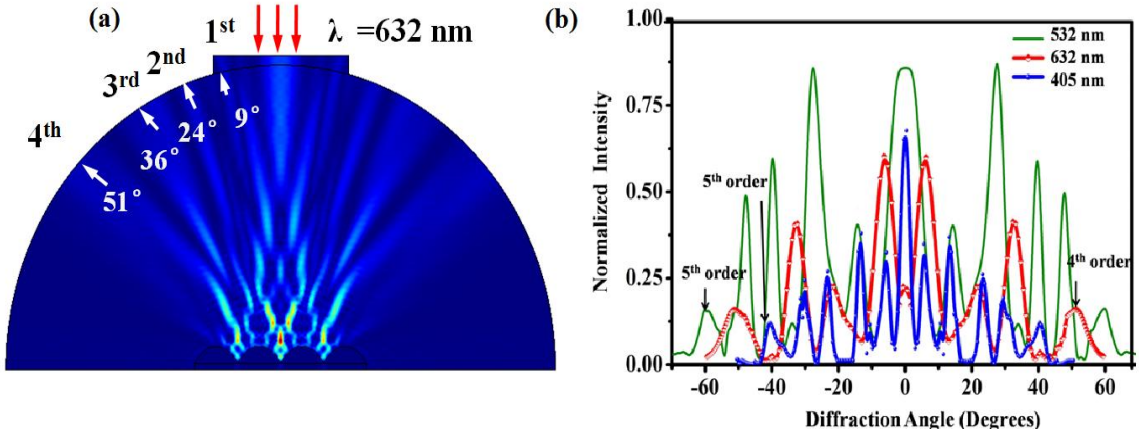

Figure 3.7 Diffraction model of the surface gratings. (a) Far-field diffraction pattern by projecting red laser. (b) Diffraction intensity plots across the hemisphere boundary as a function of angle corresponding to three incident wavelengths [60].

Fig 3.7(b) illustrates the diffraction spectra in response to red, green and violet laser beams, all diffraction spectra exhibited symmetrically diffracted spots, with red diffracted at higher angle and blue at lower angle for the same order. Four diffraction

orders were observed for red while five diffraction points were seen in response to green and blue beams. The simulated diffraction angles regarding each order and each laser beam are listed in Table 3.1.

Table 3.1 Simulated diffraction angles in response to red, green and blue laser.

	Angle from normal/zeroth order ( )				
Incident wavelength	First	Second	Third	Fourth	Fifth
632 nm (red)	6	22	33	51	-
532 nm (green)	14	27	38	47	60
405 nm (blue)	5	13	23	30	41

3.4 Optical experiments on surface grating

Based on computational simulation for diffraction pattern of ink-based grating, a series of optical experiments were performed to characterise the optical properties of ablated ink grating. A semitransparent integrating sphere setup was used to collect the diffracted spots from the surface grating hologram, the sample was aligned in the centre under the integrating sphere, the laser beam shone perpendicularly to the surface of grating. The diffraction spots were projected on the screen of hemisphere as shown in Figure 3.8.

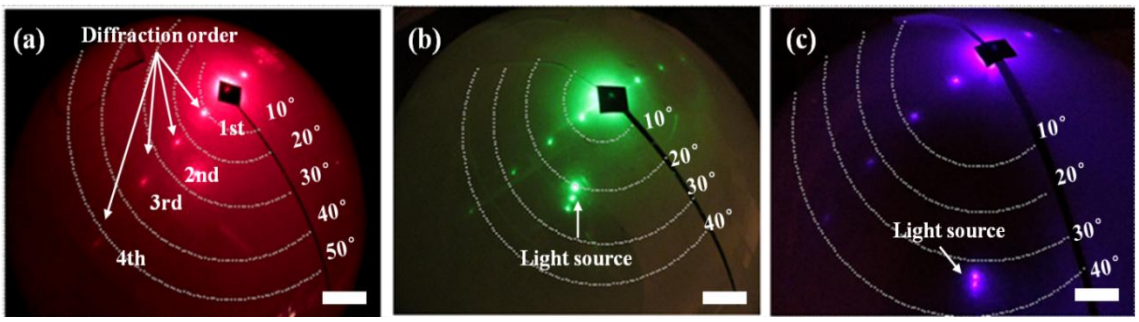

Figure 3.8 Optical characterisation of the surface grating by shining (a) red, (b) green and (c) violet light sources. Scale bar =5 mm.

Multiple diffraction orders were observed corresponding to each incident wavelength, this was due to large spacing which distributed the incident light energy into different orders. Moreover, it is found that the number of diffraction orders for red laser was coincide with simulated results (four orders), as for green and blue lasers. Only fourth order was displayed on the screen of hemisphere. In order to assess the diffraction angles for each order and the diffraction efficiency for ink-based grating, angle-resolved optical power experiment as a function of wavelength and rotation angle was conducted, the grating sample was situated in a slot of fixture, which was shone perpendicularly by incident beam from backwards, the fixture was connected with a stepping motor which was capable of rotating 360 ° by an increment of 1 °. To be identical to the integrating setup, the range of rotational angles was set from -90 ° to 90 °, an optical power meter was placed in alignment with the sample a few centimeters away. The schematic of optical power measurement setup is represented in Figure 3.9.

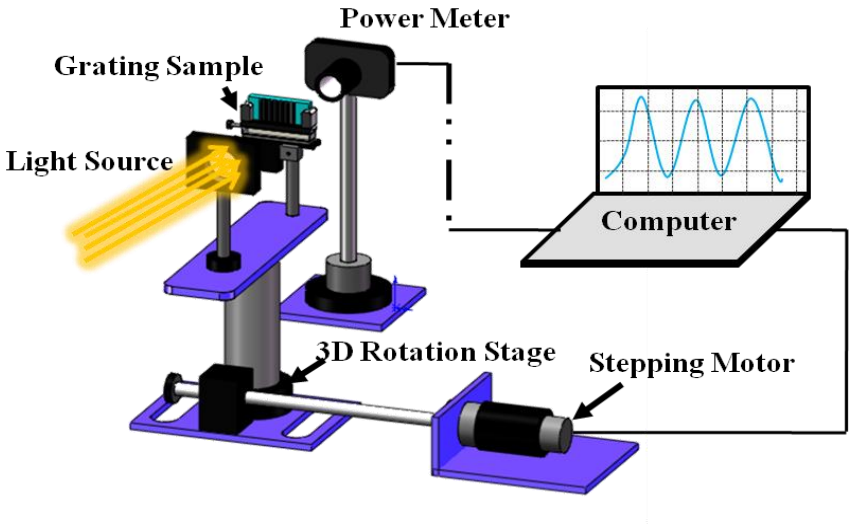

Figure 3.9 Angle-resolved measurements of the surface hologram

Figure 3.10(a)-(d) display the diffraction intensity plots corresponding to three wavelengths as a function of rotation angle. A symmetrical number of peaks were observed on each side of the non-diffracted zeroth order although there was less than 1μW distinction (<0.1%) in peak intensity between each side. The diffraction intensity plots showed that the grating had four orders under red light (12 °, 24 °, 38 °, 56 °). Five diffraction orders for green light (10 °, 20 °, 30 °, 42 °, 63 °), and violet light (7 °, 14 °, 22 °, 29 °, 39 °) were discovered in the range of 180 °, where only four orders were displayed on the screen of integrating sphere, revealing that the diffraction efficiency for the fifth order was too weak (~ 0.1 μw) to be captured on the screen. The experimental results were in good agreement with the simulated one regarding diffraction orders and angles.

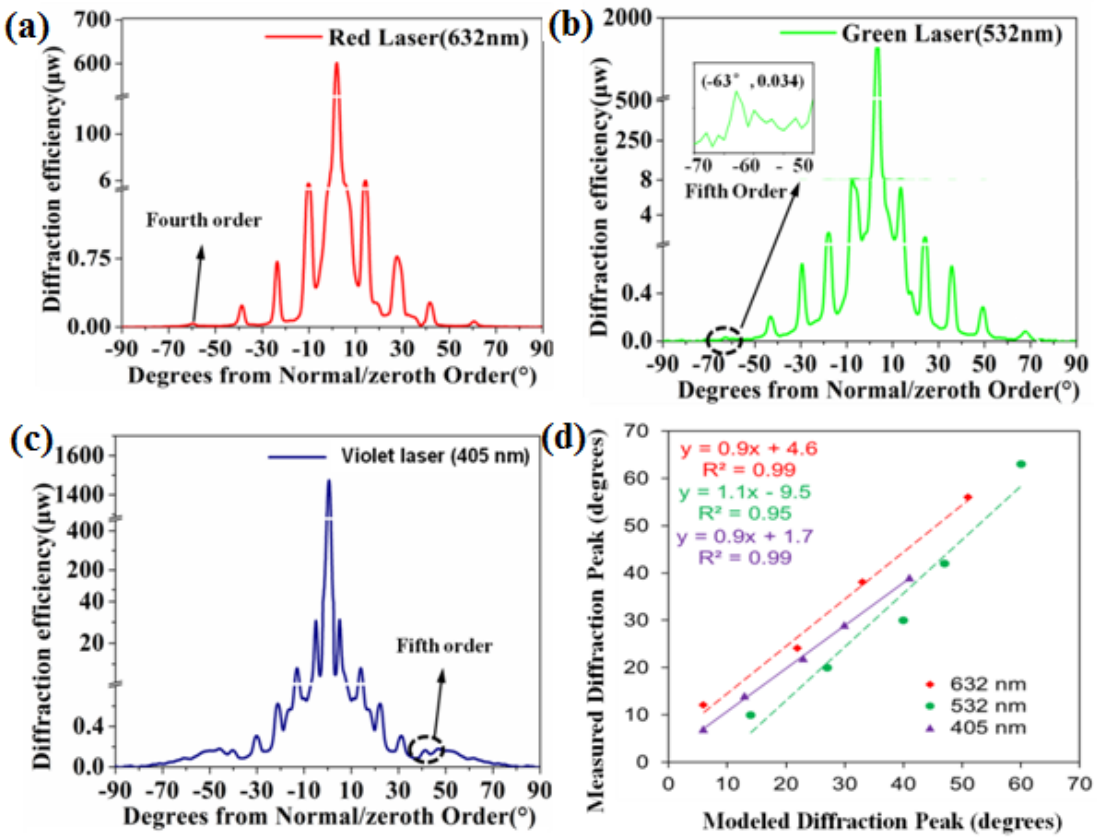

Figure 3.10 The relationship between the diffraction angle and diffraction intensity at normal incidence of (a) red, (b) green and (c) violet light. (d) correlation between the angles of the simulated and experimental diffraction peaks.

Figure 3.10(d) shows the correlation between measured and simulated diffraction peaks. The presented model allowed predicting the diffraction angles with R^2 values of 0.99, 0.95 and 0.99 for red, green and violet light, respectively. The decrease in the prediction ability for the green-violet light region may be attributed to absorption of light by the ink in this region. The experimental diffraction efficiencies were calculated by adding all scattered spots in transmissive and reflective modes. For example, in the sample illuminated by 405 nm wavelength, the total diffraction efficiency was 8.43% by adding ten (five spots from each side of normal) transmissive spots in forward direction and ten reflective spots in backward direction.

For the diffraction efficiency, ~55% and ~45% contributed to transmissive and reflective diffractions, respectively.

3.5 Conclusions

A one-step, flexible, rapid fabrication strategy for holographic recording was proposed. A thickness of 150 nm permanent ink-based hologram was prepared by a 5 ns single laser beam ablation. The whole process was completed within seconds by moving the XY translation stage to gain big ablation area.

The morphology and topography of ink-based grating was characterised by ESEM images and AFM images, well-ordered gratings were presented clearly with a periodicity of ~2.6μm. Optical characterization of ink-based hologram was subsequently performed by a batch of optical experiments, the integrating sphere showed symmetric diffraction spots which was proven by computational simulation results. However, accurate diffraction angles for each order, each wavelength (405 nm, 532 nm and 632 nm) and diffraction efficiency were determined by optical power meter setup, The diffraction angles for violet, green, and red are (7 °, 14 °, 22 °, 29 °, 39 °), (10 °, 20 °, 30 °, 42 °, 63 °), (12 °, 24 °, 38 °, 56 °), respectively. The measured diffraction angles were in line with simulated data. The total diffraction efficiency for violet illumination was calculated to be 8.43% by including all diffracted spots in the transmissive and reflective modes.

It can be concluded that single laser beam interference strategy have great potential in making optical holograms for rapid production, flexibility and low cost.

4. Holographic Fabrication of Nanophotonic Devices

4.1 Introduction

A asymmetric Fresnel zone plate with a 4 nm thick golden layer (focusing device) was fabricated and presented in this chapter using the single laser beam strategy introduced in chapter 3.

Fresnel zone plate has attracted attention from researchers all over the world for its unique characteristics such as high numerical aperture (NA) [61], compact volume and low weight [62-64], and high resolution imaging [65,66] in X-ray and extreme ultraviolet conditions.

Unlike traditional optical lens or curved mirrors, a zone plate focusing light beams by diffraction instead of reflection or refraction, it is composed of radially symmetric rings which alternate between opaque zones and transparent ones [62]. It is the constructive interference between opaque and transparent occurring at the focal point that forms the strong intensity of image. The radius of each zone for a zone plate is formulated as equation 4.1 [67].

$$R_n = \sqrt{n\lambda f + \frac{n^2\lambda^2}{4}} \tag{4.1}$$

where R_n is the radius of n-th zone, and f is the focal length at which the image or spot is focusing, λ is the light beam hitting on the zone plate, when the focal length f is far bigger than the zone plate, equation 4.1 can be written as [67]:

$$R_n \approx \sqrt{nf\lambda} \tag{4.2}$$

In the limitation of long focal length, the area of each zone should be approximately the same, and the width of each zone should decrease further from center to outer edge. An example structure of symmetric zone plate is shown in Figure 4.1(a), and the focal point is clearly shown along the propagation of incident beam as shown in Figure 4.1(b).

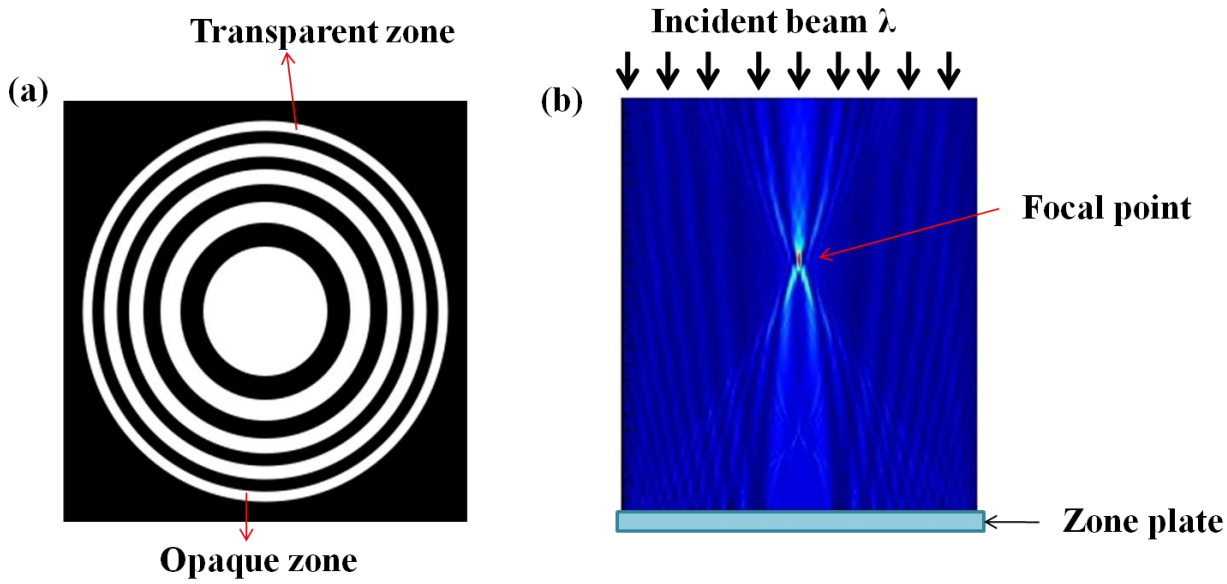

Figure 4.1 Construction of a flat zone plate. (a) Typical binary zone plate consisting of "black" (opaque) and "white" (transparent) zones. (b) 2D simulation of focusing effect by symmetric zone plate.

4.2 Holographic Gold-based Gratings

Before preparing the zone plate sample, surface gold grating was fabricated via the same setup. For fast production, the gold was evaporated over a microscope glass to obtain an average thickness of 4.5 nm with a transparency of ~50%, the absorption peak for gold of this thickness overlapped with the laser beam (λ=532 nm) used to

produce the grating.

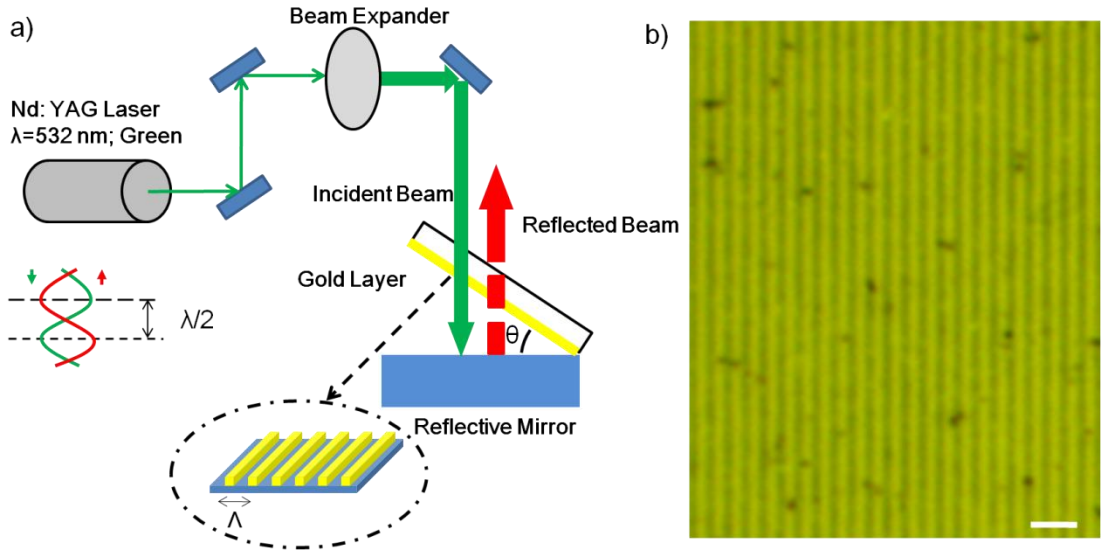

Figure 4.2 Fabrication of the holograms through nanosecond laser light interference. (a) Schematic of surface grating recording setup. (b) Microscope image of gold surface grating showing periodic surface gratings. Scale bar = 2μm.

Figure 4.2(b) displays the well-ordered periodic grating produced by single 532 nm laser beam within seconds. The spacing was measured to be 820 nm at a tilt angle of 20 °. According to the equation provided in eq.(3.2), theoretically, the periodicity should be 778 nm. The difference may be attributed to the simplicity of the laser setup and errors in determining the inclined angle (see Appendix A for detailed information). Similar to what was measured for ink-based grating, the diffraction patterns for gold-based grating was observed by projecting white light source, green laser, and red laser, respectively. The diffraction spots were exhibited on the screen of a semi-transparent integrating sphere (r =15 cm).

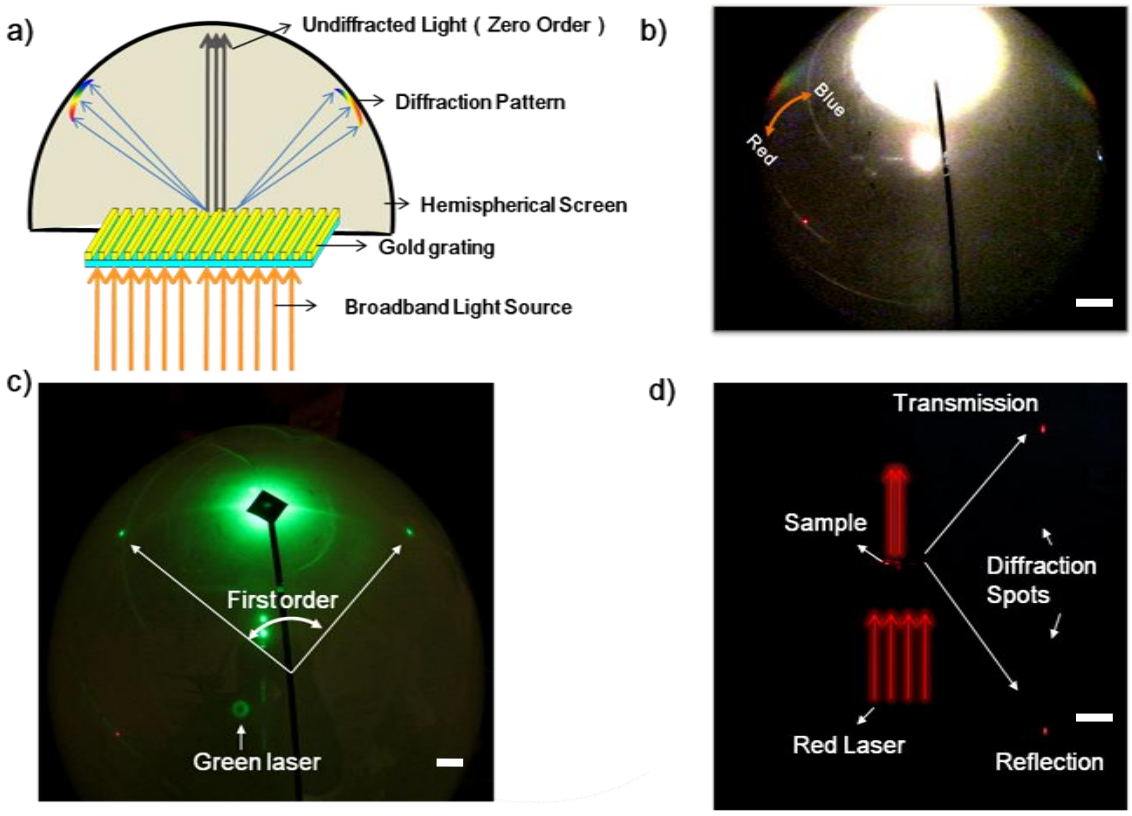

Figure 4.3 Optical characterization of gold-based diffraction grating. (a) Schematic of a integrating sphere. (b) Continuous diffracted spectrum by white light source illumination. Scale bar = 2 cm. (c) Diffraction spots in transmission mode by shining green laser. Scale bar = 2cm. (d) Diffraction spots displayed on a plane screen. Scale bar =3 cm.

As shown in Fig. 4.3(b), a well-ordered diffraction rainbow was observed by inducing a broadband white light source, with blue at a lower degree and red at a larger degree, which matched with the diffraction equation. As for monochromatic light, the diffraction pattern was concentrated spot rather than a broadband ribbon, as shown in Fig. 4.3(c). In addition, the diffracted spots in both transmission and reflection mode were visualised using flat screen placed beside the sample, it is obvious that the diffracted spots for both modes situated symmetrically from the

zeroth order (non-diffraction portion) of incident red beam.

Specifically, the exact diffraction angle and power for each individual monochromatic laser source were studied, the power meter setup was similar to the measurement device for ink-based grating. The difference was that the power meter was placed much nearer (~5.4 cm) to obtain sufficient energy of diffraction for the sake of 5 nm thickness of gold layer. The schematic of measurement setup is shown in Figure 4.4(a):

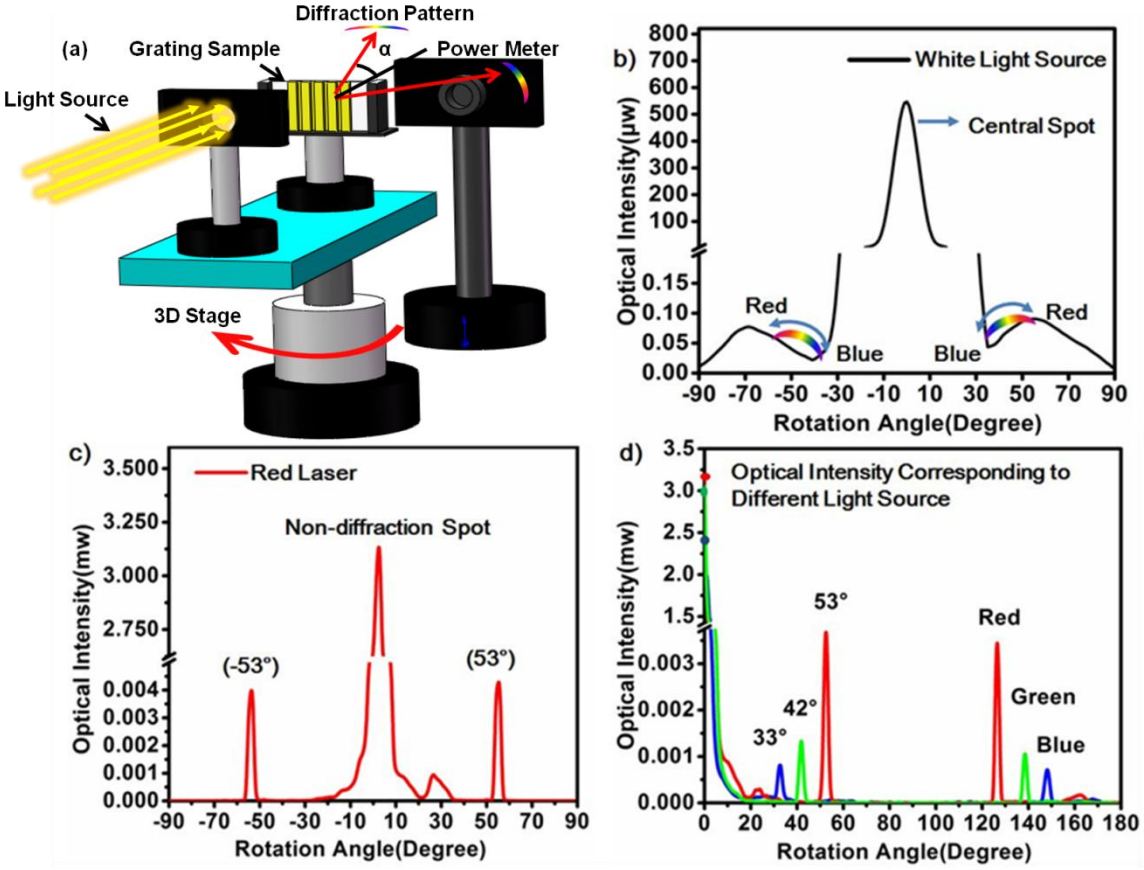

Figure 4.4 Angle-resolved measurements for gold-based grating (a) Setup for the measurements of the optical intensity. (b) Optical intensity distribution by normal incident white light. (c) Diffracted optical intensity distribution by red laser (650 nm) illumination. (d) Diffracted optical intensity distribution in response to blue (440 nm), green (532 nm) and red (650 nm) wavelengths.

Figure 4.4(b)-(d) plots the diffracted optical intensity distribution as a function of 180 ° rotation. Two broadband peaks (from 35 ° to ~60 °) were observed symmetrically from the undiffracted zeroth order, where the diffraction pattern was in agreement with what was seen in Fig. 4.3(b), the optical intensity plots in response to red (650 nm), green (532 nm), and blue (440 nm) were shown in Fig. 4.4(d), the transmissive spots and reflective spots were situated symmetrically with mostly the same power, with blue diffracted at lower angles and red at higher angles. The first order diffraction angles for blue, green and red were measured to be 33 °, 42 ° and 53 °, respectively, which correspond to the theoretical grating equation (Eq.3.2). The diffraction efficiency corresponding to red beam (Fig.4.4(c)) can be calculated to be 0.54% by adding four diffraction spots (two spots in transmission mode and the other two in reflection mode) together, both transmission and reflection diffractive spots contributed equally to the total diffraction efficiency.

4.3 Asymmetric Zone Plate

Based on the fabrication of ink-based and gold-based surface holographic gratings, a focusing device (zone plate) was demonstrated using the single nanosecond laser ablation strategy, the recording setup is depicted in Figure 4.5.

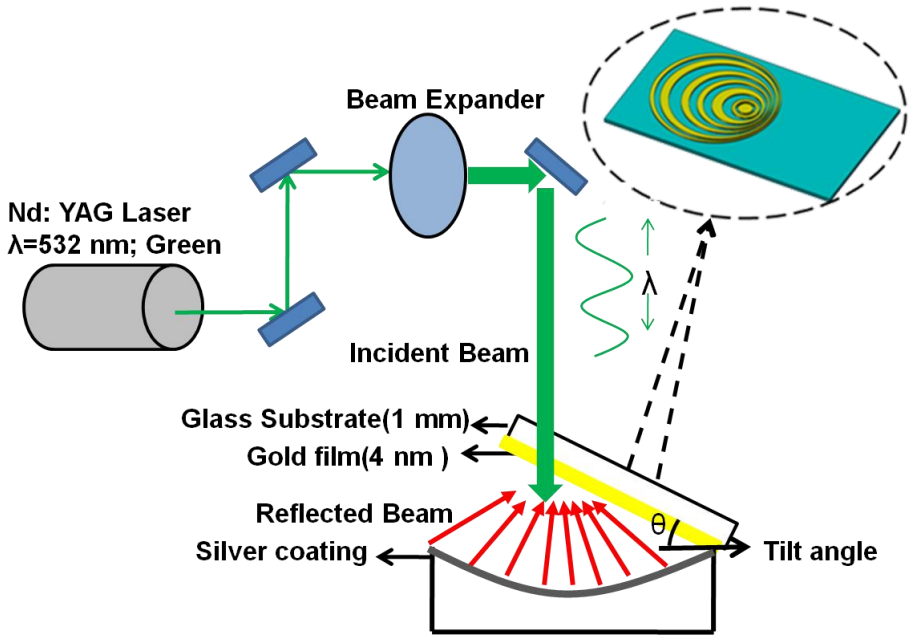

Figure 4.5 Schematic setup of surface hologram recording system.

In this recording setup for holographic zone plate, the object was changed by a concave mirror instead of a plain object. A concave mirror has a reflecting surface which bulges inward (away from the incident light) to converge light to a focal point. The diameter and radius of curvature of concave mirror were 25 mm and 62 mm, respectively. A thin silver coating was deposited on the surface of concave mirror, which had a high reflectivity of 90%, and thus a strong interference pattern occurred between the collimated incident beam and multiple beams reflected from the concave mirror. During the recording process of zone plate sample, the recording substrate was tilted by 30 ° from horizontal plane, this was to get an uneven intensity distribution from the interference pattern.

To study the intensity distribution produced by the interference of multiple laser beams throughout the concave mirror, a computational simulation was performed

using finite element method (FEM) by COMSOL Multiphysics. Due to the large computational memory and simulation time required for the real size of actual model, the boundary condition was set to be scattering to avoid any reflection from the boundary. A 2000 times minification of original concave mirror was designed and modelled (the radius of curvature was 11μm and the diameter was set to be 12μm), the curved surface was chosen to be silver with a refractive index of 0.053 at 532 nm incidence, and the remaining parts of concave mirror was set as silica glass with a refractive index of 1.47. In this simulation, a 2D model was set up and the electromagnetic field with wavelength of 532 nm was induced to obtain interference pattern as shown in Figure 4.6(a).

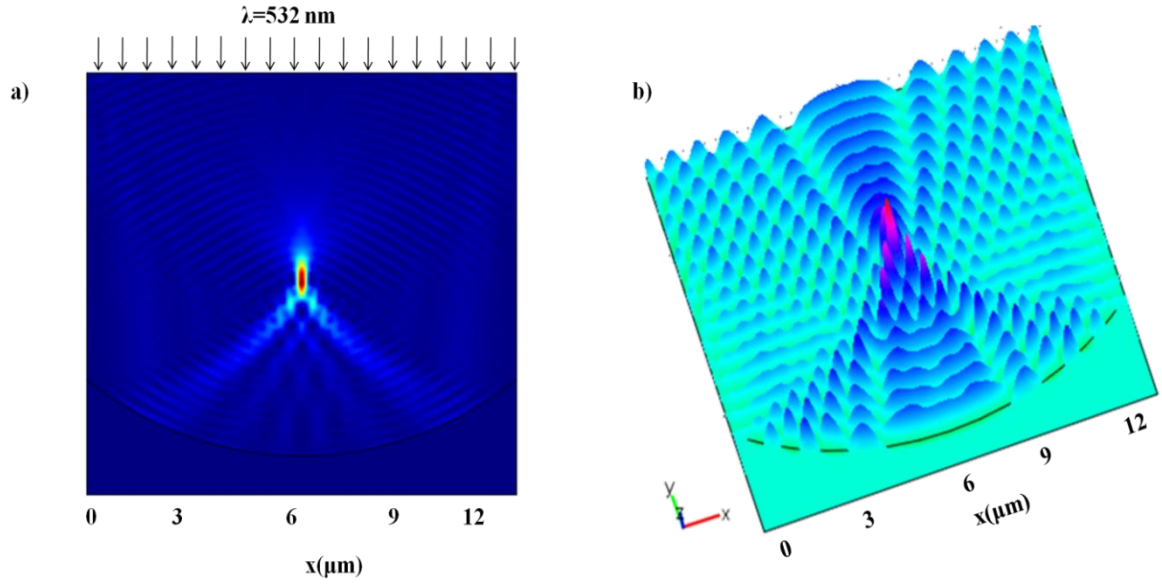

Figure 4.6 Simulated interference pattern. (a) Electromagnetic intensity distribution in response to green laser beam (λ= 532 nm). (b) the 3D representation of electric field propagation showing the focusing effect, where circular peaks are observed.

Figure 4.6(a)-(b) show notable focusing spot among the intensity distribution, which was identical to the converging effect by concave mirror. In addition, the well-ordered circular interference pattern indicated the intensity distribution of a normal zone plate.

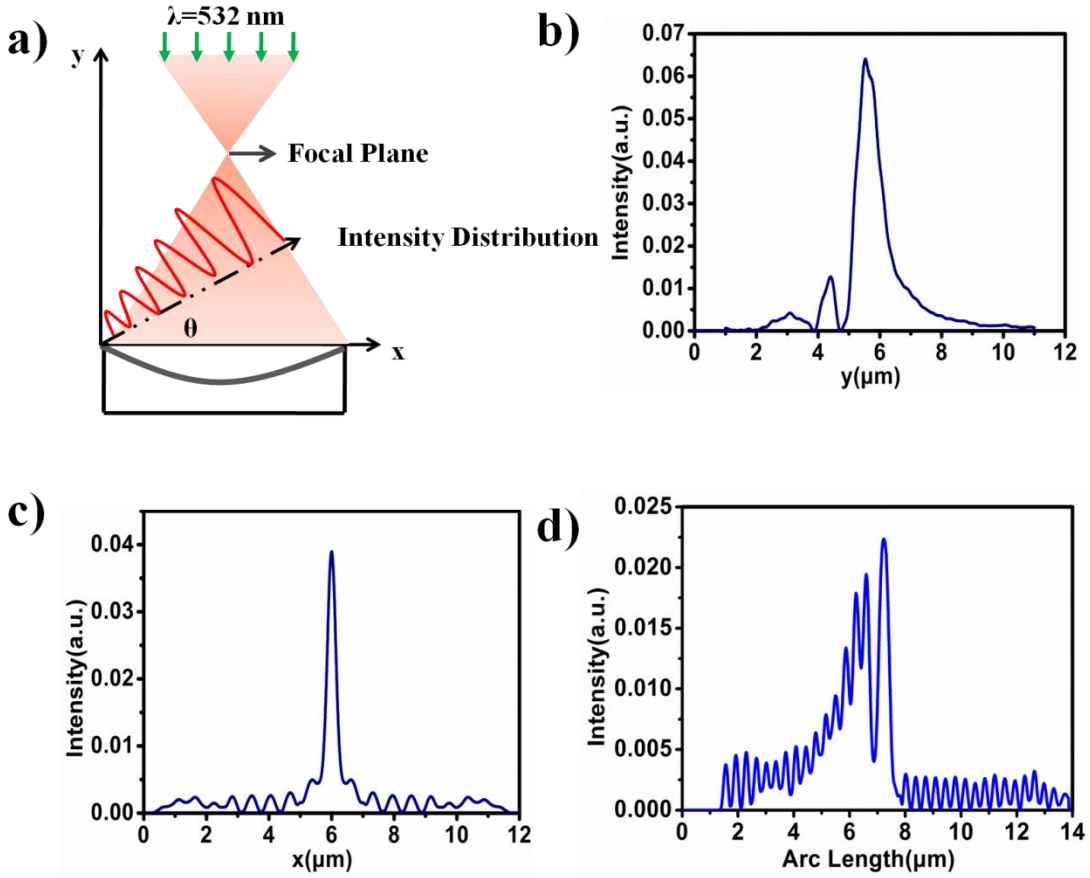

Figure 4.7 Intensity distribution of electromagnetic field plotted at different planes. (a) Illustration of interfering pattern at focal plane and the tilted plane. (b) Intensity plots along the y axis and (c) X axis at the focal plane. (d) Intensity distribution at the tilted plane of 30 °.

The interfering intensity distribution at focal plane as well as the 30 ° tilted plane were also simulated as shown in Figure 4.7(b)-(d), the focal length was simulated to be 5.5 μm according to Fig. 4.7(b) under the geometry of concave mirror with a radius

of curvature of 11 μm. According to Snell's law, the focal length for a typical concave mirror can be defined as half of the radius of curvature regardless of any focus errors, the simulated result was in great agreement with the theory. Figure 4.7(c) shows the intensity distribution along x-axis at the focal plane, and a high intensity focal point was observed. The profile was symmetrical about the focal point. In contrast to the uniform distribution of intensity at focal plane, the interfering optical intensity at the 30 ° tilted plane showed asymmetric power distribution from the centre of concave mirror, as depicted in Fig. 4.7(d), the intensity of constructive interfering peaks decreased from one side to the other side. This asymmetric interference pattern, when used for ablation of a thin gold film, produces an asymmetric zone plate.

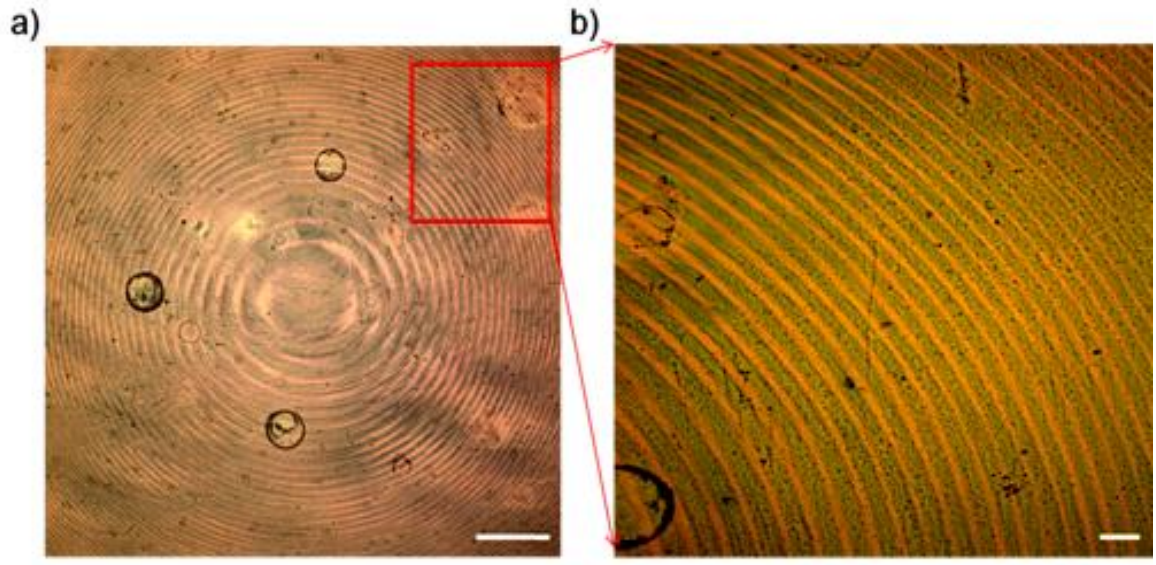

Figure 4.8 Microscopy images taken by "Alicona" system. (a) Overall image of gold zone plate sample. Scale bar = 200 μm. (b) Localized and magnified image of selected portion from (a). Scale bar = 20μm.

The dimensions and surface morphology of ablated zone plate was further determined by using optical microscopy and AFM characterization, the overall and

localized images of zone plate sample were clearly seen under the magnification of 100 times, as shown in Figure 4.8. A plate with radial zones alternating from gold circles (opaque zones) to transparent zones (substrate) was visualised in Fig.4.8(a), the radius of the outmost zone was measured to be around 2 cm, Figure 4.8(b) showed the magnified region selected from Fig. 4.8(a), suggesting that the width of zones decreased farther from centre to the edge, varying from 100 μm to few hundred nanometers, the dimensions of zones were patterned so that the diffracted light constructively interfered at the desired focus, creating a strong image there.

The surface morphology focusing on a typical zone was analyzed using AFM characterization, the images are shown in Figure 4.9.

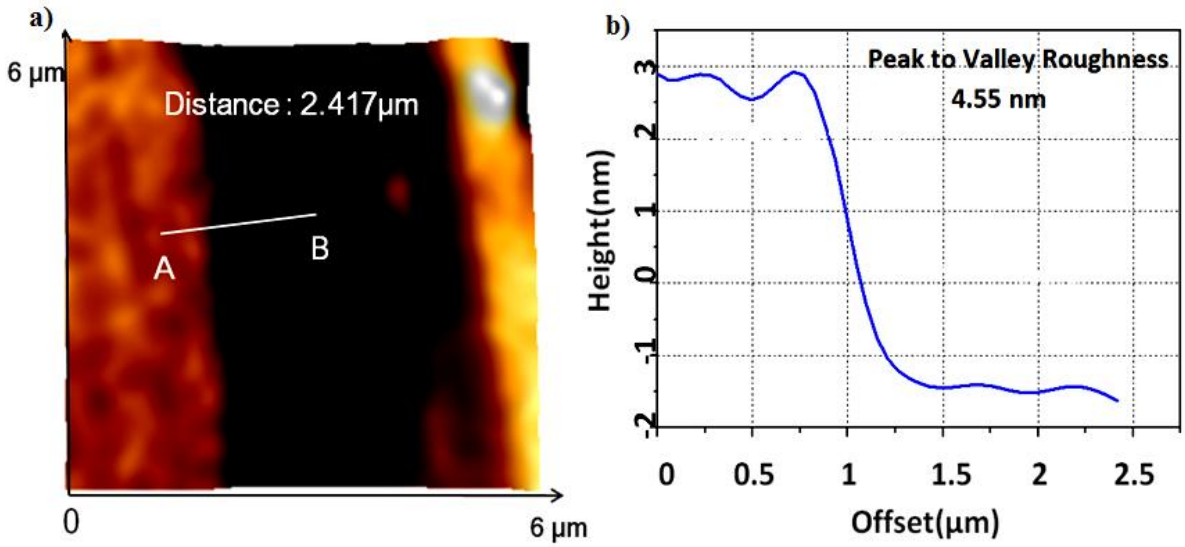

Figure 4.9 AFM characterization of the holographic FZP fabricated via laser ablation. (a) Profile for a gold- substrate outer zone. (b) Height profile of segment AB from panel (a).

Figure 4.9(a) exhibits a zoomed out zone where both transparent part and gold part existed. Point A and B represented the golden part and the transparent part,

respectively, the height distribution ranging from gold layer to substrate is plotted according to Figure 4.9(b). It is shown that the average height (thickness of golden layer) was 4.55 nm and a side wall tilt was observed at the gold-substrate transition boundary.

4.4 Experimental Analysis and Discussions

To investigate the optical characteristics of ablated asymmetric zone plate sample, a series of optical experiments were conducted, the diffraction pattern was shown by shining a broadband white light source vertically upon the gold-based lens, the experimental equipment is shown in Figure 4.10.

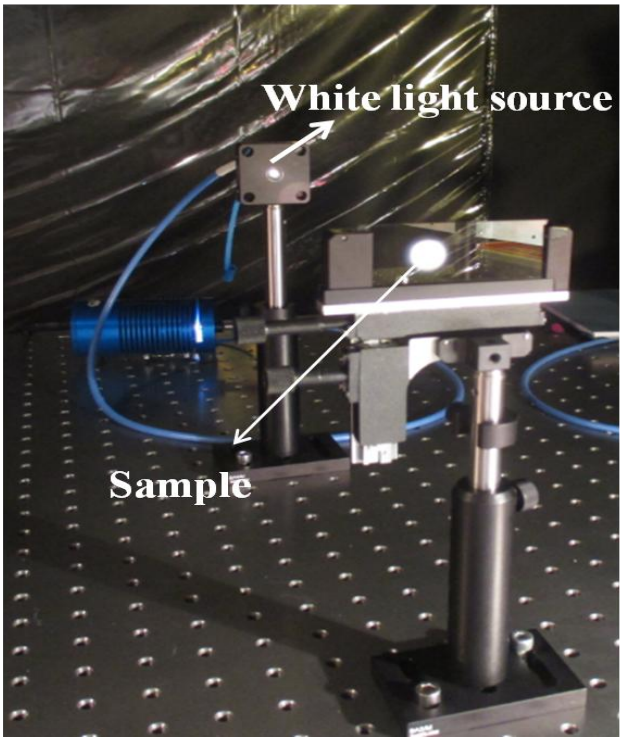

Figure 4.10 Experimental setup for illumination upon the surface hologram.

Significantly different from conventional zone plate which focuses incident ray along the optical axis, the diffraction image showed a special diffraction angle α with

respect to incident direction, this differentiated the diffraction image away from the strong undiffracted background (zeroth order). The diffraction pattern was well-ordered rainbow in high contrast ranging from blue to red as shown in Figure 4.11. Both transmissive and reflective diffraction pattern were situated symmetrically on each side of the gold- based focusing lens.

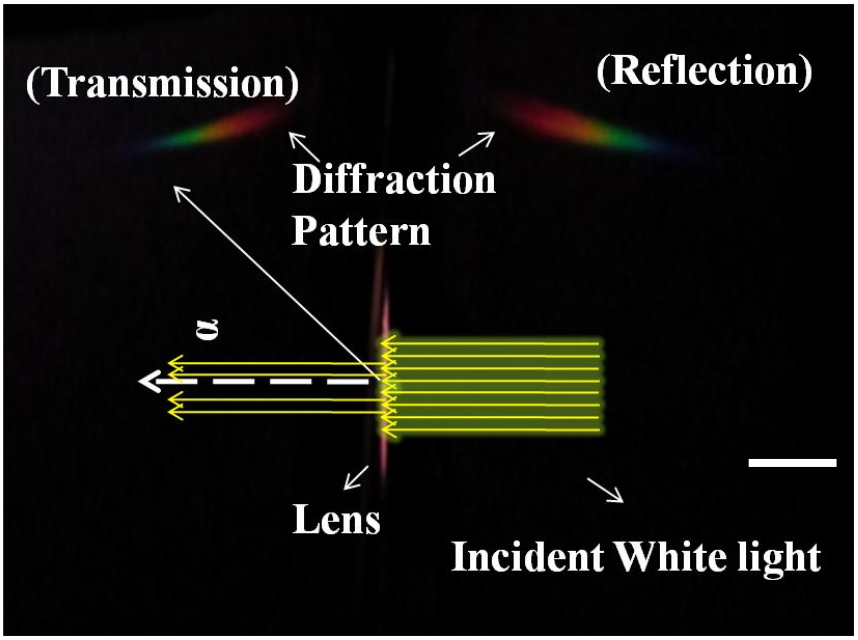

Figure 4.11 Camera images of diffraction rainbow produced by gold-based zone plate under illumination of broadband white light source. Scale bar = 5 cm.

In order to figure out the accurate diffraction angle for ablated asymmetric FZP sample as well as the focal length for each individual incident beam in the regime of visible light, the angle-resolved spectrometer experiment was performed and the schematic of spectrometer device is plotted in Figure 4.12.

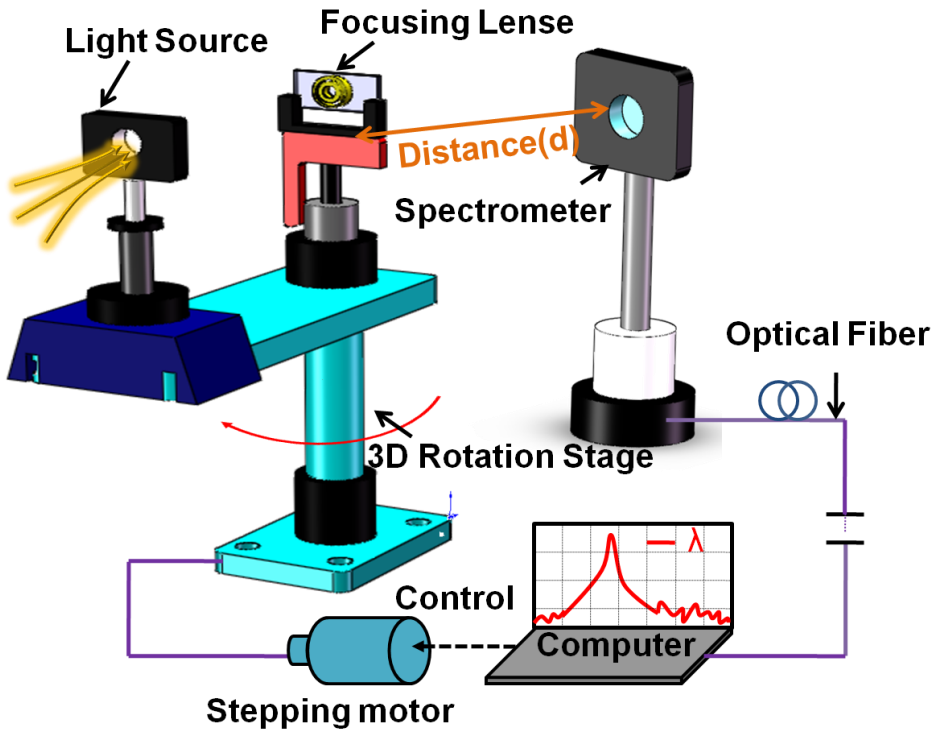

Figure 4.12 Angle-resolved measurement setup for the Fresnel zone plate.

The sample was mounted and fixed in a straight slot which was in alignment with the holder of the light source, and thus the incident light could hit on the sample perpendicularly. The slot and holder was supported on a 3D adjustable stage which was connected to a stepping motor, the stepping motor was capable of controlling the 3D stage to rotate in the range of 360 ° with a minimum increment of 1 °. Other than that, a spectrometer was placed in front of the focusing lens to capture the diffraction spectra at different angles, the distance between the spectrometer and the sample (d) was varied from 8.7 cm to 21.8 cm in order to detect the focal lengths for different wavelengths.

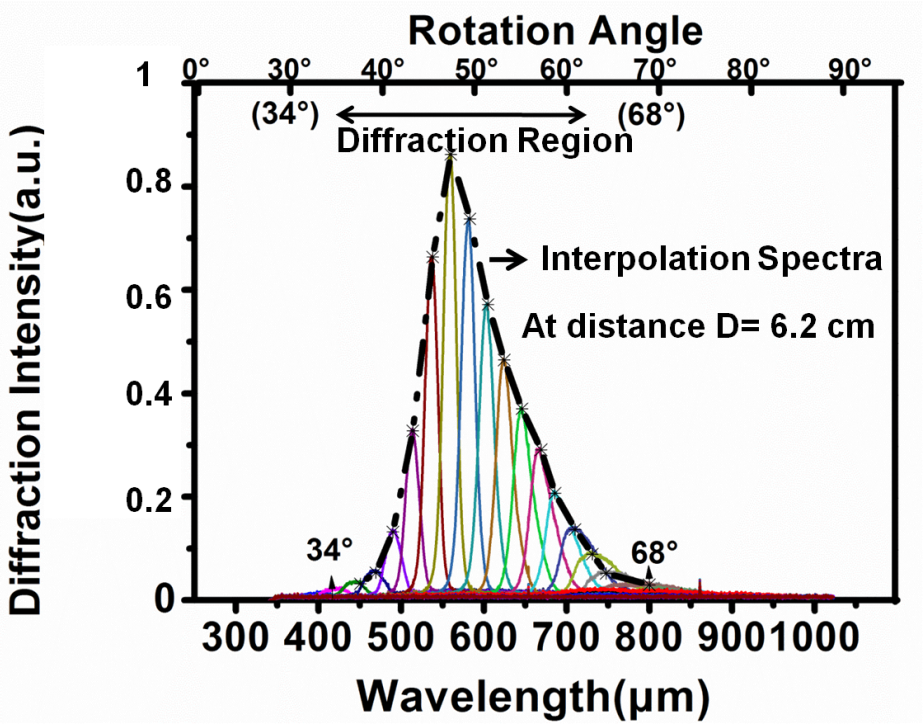

Figure 4.13 Diffraction spectra obtained from a broadband white illumination

Figure 4.13 plots the diffraction spectra at the distance of 6.2 cm as a function of rotational angle, the diffracted spectra ranged from 400 nm to 800 nm which showed a broad diffraction angle ranging from 34 ° and 68 °. Each spectrum was obtained at intervals of 2 °rotation. To obtain continuous diffraction spectra throughout the whole diffraction rainbow, an interpolated curve was generated by connecting the peak intensity of each spectrum. It can be inferred that the optical intensity for green light region (492-577 nm) was the strongest among the diffraction spectra.

The focal lengths in response to three typical wavelengths (455, 532 and 650 nm) were studied by measuring different diffracted intensities according to a series of distances between the sample and the spectrometer. For wavelength of 532 nm, the diffraction intensity was higher than that of 455 and 650 nm, which was supported by

Fig.4.13. The maximum diffraction intensity was observed to be around 11.2 cm, which was the experimental focal length for the wavelength of 532 nm (green light). In terms of blue light, the optical intensity increased all the way up to 13.7 cm and then dropped down dramatically to minimum intensity at the distance of 21.2 cm, suggesting that the focal length should be ~13.8 cm. Different from the regularity seen from green and blue lights, the diffraction intensity for 650 nm in red decreased when the distance was increased, showing a focal length of ~6.2 cm.

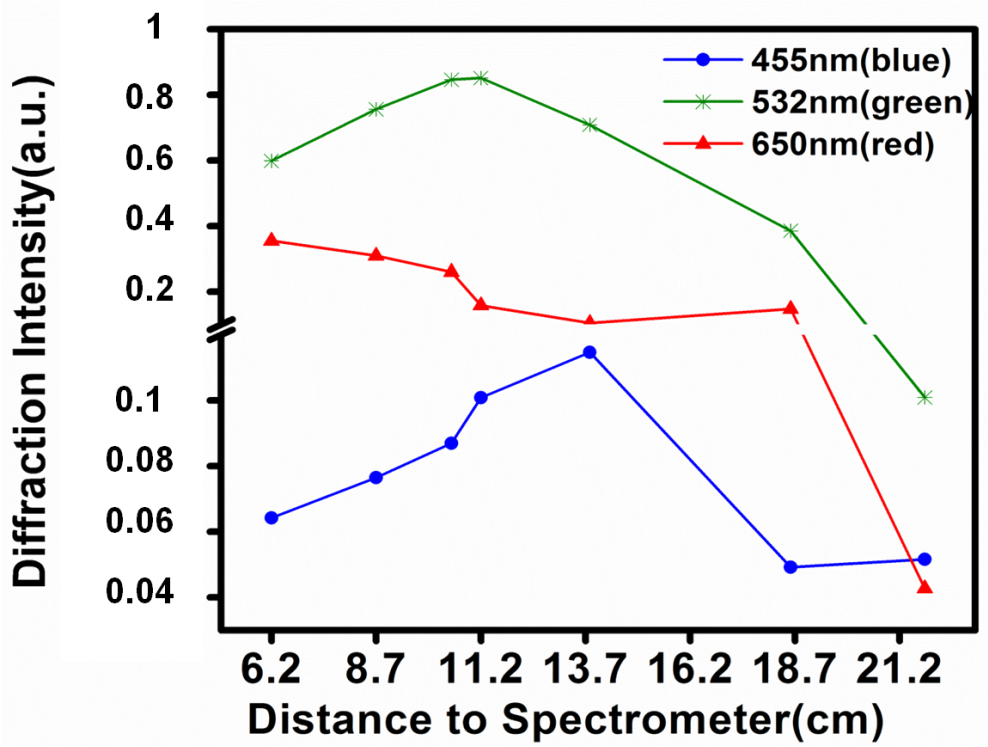

Figure 4.14 Normalized diffraction intensity in response to blue, green and red light.

The diffraction efficiency was subsequently measured by optical power meter setup, the optical power meter was positioned at a distance of 18.3 cm away from the

gold FZP sample, the intensity plot was recorded as a function of rotational angle is shown in Figure 4.15.

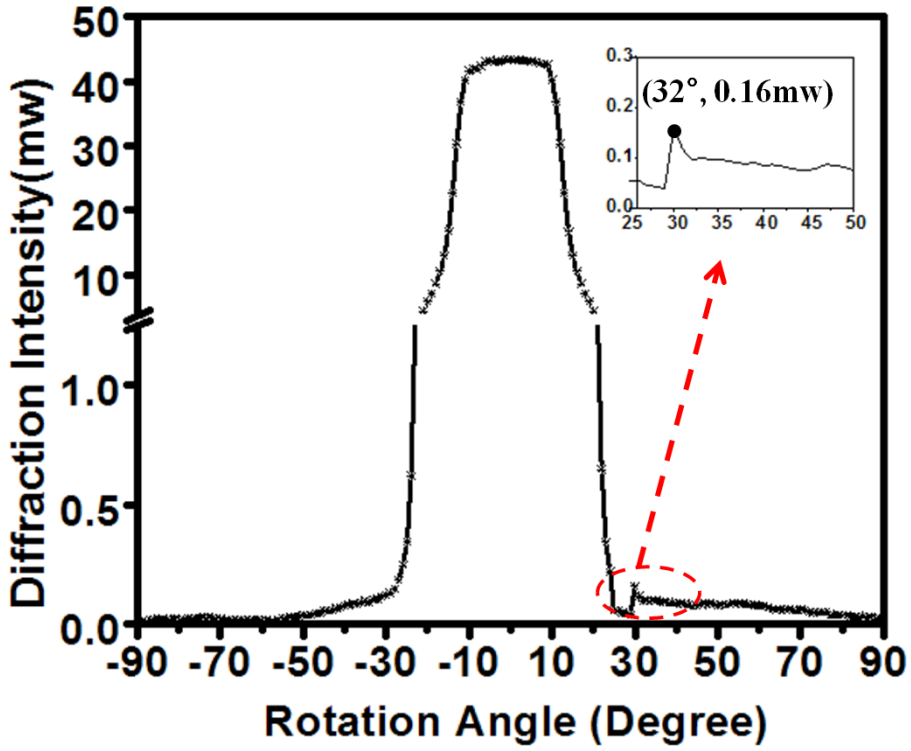

Figure 4.15 Diffraction intensity distribution it as a function of 180 ٩otation

It is observed that there was broadband peak intensity around 0 ° in the centre of the intensity plot, and there was another small peak intensity at the angle of 32 ° after the presence of the broadband white light source, indicating the diffraction pattern in transmission mode. This coincided with the image of diffraction rainbow demonstrated in Fig. 4.11. Additionally, there was another diffraction peak in reflection mode in backwards direction, which was out of the range of measured angles. The maximum diffraction efficiency for white light illumination was

calculated to be 0.8% by adding two symmetric diffracted spots together (~0.4% contributes to each spot).

4.5 3D Holograms *via* Laser Ablation

As demonstrated in previous chapters, surface holographic gratings as well as asymmetric zone plates were successfully fabricated within seconds. The prepared holographic samples exhibited well-ordered and legible diffraction pattern under illumination of different light source.

Hereby, some other holographic samples are presented to further demonstrate the application of single nanosecond laser beam ablation strategy on making holographic devices. The following image is a quick response code printed on a transparent substrate.

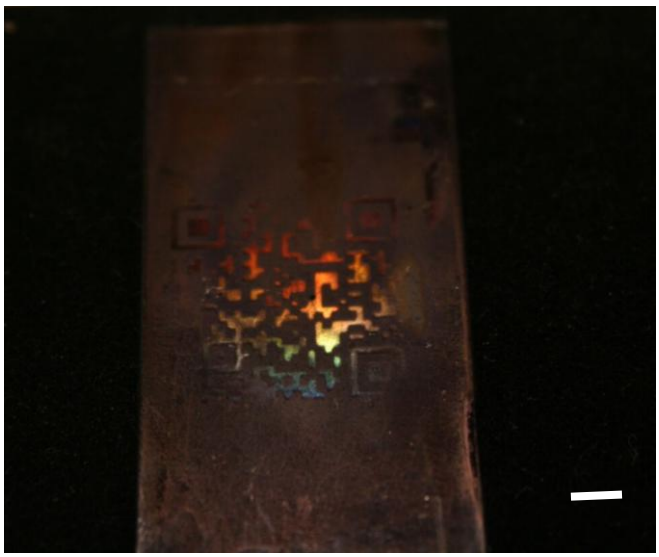

Figure 4.16 3D holographic printed QR code. Scale bar = 2 cm

The QR code can be applied to authentication and security identification for companies to distinguish internal staff from external people. Also, the end user can use smartphone to decode the hologram to allow access to personal information.

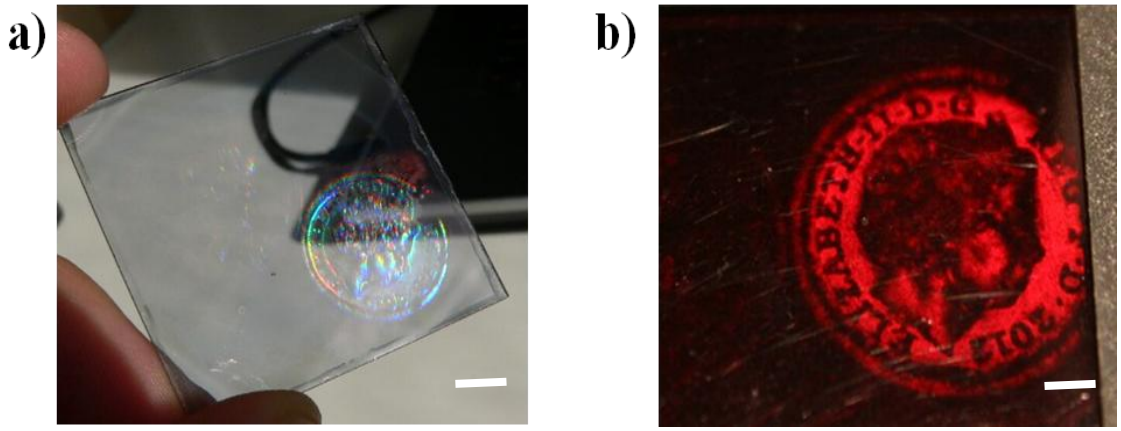

Figure 4.17 3D holographic coin recorded by single nanosecond laser interference. The image of coin is reproduced by shining (a) white light source, scale bar = 1cm and (b) red laser beam. Scale bar =0.5 cm.

Figure 4.17 illustrates the holographic coin image made by single laser beam, the fabrication setup used to make this sample was in accordance with the one depicted in Fig. 3.1. The only difference was that the flat transparency was replaced by a real coin to enable the wavefronts of object beam which hit on the coin to be recorded. The coin hologram displayed polychrome pattern when illuminated by white light, however monochromatic virtual coin images could be constructed when illuminated with a laser beam, Fig. 4.17(b) displayed a red coin image when shining with red laser. Another application is represented by a handwritten signature hologram, the signature was written on a pressure-sensitive tape, and then was used to fabricate the hologram, the signature hologram is shown in Figure 4.18.

Figure 4.18 Ink-based Holographic signature

This handwritten hologram may be applied to personal characterization and 3D artworks of handwriting.

4.6 Conclusions

In this chapter, gold-based surface grating hologram as well as asymmetric focusing device were fabricated corresponding to the technique of single laser beam ablation.

The gold-based grating showed well-ordered fringes under100x magnification of microscope, the periodicity was measured to be 820 nm, which was in good agreement with the theoretical equation 3.2. In addition, integrating sphere experiment was performed and well-ordered diffraction rainbow in both transmissive and reflective modes, the diffraction efficiency was measured to be 0.54% for incident read beam by the optical power meter measurements.

In terms of asymmetric zone plate hologram, the alternate zones between gold

and substrate were clearly showed by microscope image. The dimensions for each zone varied from 100 μm in the centre to few hundred nanometers in outer regions. The thickness and surface topography were further characterized by measurements of AFM, the average thickness was 4.55 nm and a side wall tilt was observed at gold-substrate boundary.

In addition, when the asymmetric FZP was illuminated with white light source perpendicularly, it showed specific diffraction angle of 32 ℃for focused image, which significantly separated the focused image from the strong background brought by incident white light beam, the focal length for three typical wavelengths were analysed by conducting the angle -resolved spectroscopy experiment. Experimental results showed that the focal lengths for blue (455 nm), green (532 nm) and red (650 nm) were 13.7 cm, 11,2 cm and 6.5 cm, respectively. The diffraction efficiency for white light illumination was determined by optical power meter experiment, the total diffraction efficiency was calculated to be 0.8% by adding two diffracted spots in reverse directions.

Furthermore, several examples of other 3D holograms were presented to demonstrate the utilization of nanosecond laser ablation technique, including 3D coin, personalised handwriting and quick response code. These holograms had a broad application prospect in either 3D artwork display or optical devices such as optical data storage, personalised authentication, security and sensing.

5. Conclusions

This thesis presents the research work to develop an efficient approach to fabricate various holograms. The proposed strategy of recording holograms was simple, time-saving, reliable and can be used for ablating a myriad of materials and substrates.

The single laser ablation setup was conducted based on the Denisyuk" reflection" mode, the surface grating holograms, as well as other 3D holograms, were fabricated using single 5 ns laser beam interference, the energy of laser beam was ~10 mJ with central wavelength of 532 nm, the ablated area was 1 cm^2 by 5 ns time, and thus bigger ablated region can be achieved under a few seconds.

Permanent ink-based grating with a thickness of ~150 nm was introduced and fabricated according to chapter 3. The theory for standing wave interference was presented and computational simulation was performed to predict the spacing of grating. As a result, well-ordered ink grating was formed by a tilted plane of 6°. ESEM and AFM characterization showed an average periodicity of ~2.6 μm, the value of spacing was in good agreement with the simulated results. Multiple diffraction orders were observed by shining different monochromatic beams vertically to the ink-based grating and the blue beam diffracted at lowest angle, followed by green and red beams. This regularity was in accordance with the diffraction theory. Furthermore, optical power meter experiment was conducted and the diffraction

efficiency for the blue beam was calculated to be 8.43% by including all diffracted spots in both transmissive and reflective modes.

Gold-based grating and FZP holographic samples were fabricated and represented in Chapter 4. The thickness of gold was merely 4 nm compared to 150 nm thick ink. The periodicity of gold-based grating was measured to be 820 nm by tilting the recording substrate by 20°, the diffraction pattern for gold based grating was well-ordered rainbow ranging from 35° to 60°, the diffraction efficiency for gold-based grating was only 0.54% for red beam due to ultrathin film coating.

The asymmetric zone plate was fabricated by interference of multiple reflected beams provided by a concave mirror and an incident beam. Simulation results of interference showed circular fringes which can be used to produced conventional zone plate. By tilting 30° for the recording plane, uneven intensity distribution was created and resulted in asymmetric zone plate. Through AFM characterization and microscope images, the dimensions of FZP was determined and the diameter of outmost zone was ~ 2 cm, and the width of the outmost zone was just few hundred nanometers. The diffraction performance of asymmetric FZP displayed well-ordered rainbows in high contrast at a diffraction angle of 32°, which was differentiated from the non-diffracted incident beam. By rotational spectroscopy experiment, the focal lengths in response to blue (455 nm), green (532nm) and red (650 nm) were 13.7 cm, 11,2 cm and 6.5 cm, respectively. The diffraction efficiency for incident white light was measured to be around 0.8% obtained from optical power meter measurements.

Other holographic devices were also demonstrated in the end of chapter 4, including 3D coin, personalized handwriting and quick response code. These optical holograms were also accomplished by single nanosecond laser ablation.

Overall, from the versatile holograms presented and demonstrated in the thesis, the strategy of ns laser interference recording of surface holograms is confirmed to be efficient and feasible to fabricate a variety of surface holograms, ranging from flat transparencies to curved or arbitrary opaque substrates (silicon-based or metallic coating). Also, a diversity of materials can be applied to achieve better resolution and high efficiency such as inks, dyes, nanoparticles, and metallic coatings. The presented approach may be applicable for printing responsive materials holograms and sensors. They also hold potential for integration with smartphone applications for the interpretation and verification of colorimetric data. This single laser interference methodology is time-saving, easy-to-fabricate, and economic, leaving out complicated alignment process and additional labor input. The fabricated multiple showing potential in numerous optical devices for personalised identification, security, data storage, and 3D artworks.

6 Future work

While the present research work exhibits great potential in optical application and can be employed to mass production. However, there are still lots of work which can be carried out in the future to produce holograms in better quality and higher efficiency.

First of all, gold was selected to be recording medium for surface grating hologram and asymmetric zone plate hologram. Though it has good absorption with incident laser, it doesn't have strong affinity to glass, which can affect the diffraction performance. This can be improved by functionalizing the surface with silane chemistry or coating the patterned surface with hydrophobic polymers. The diffraction efficiency can also be increased by increasing the thickness of deposited layer and using materials with a high refractive index.

Furthermore, the simulation model for predicting the periodicity of grating was simplified, without considering the refracted beam at the ink-air interface. A more accurate geometry may be built up to analyze all coherent beams to get more accurate interference parameters.

Finally, due to the complexity of dimensions of asymmetric zone plate, the simulation of asymmetric zone plate remains undone, the simulation of ablated zone plate sample can give direct illustration of focusing pattern and the simulated focal length for any incident wavelength. In addition, the FZP with arbitrary diffraction

angle can be fabricated if the dimensions for FZP can be preset by simulation of asymmetric zone plate.

With the rapid development in holographic industry and the increasing applications for optical devices, it is believed that more and more efficient holographic recording methodologies will be put forward and versatile materials can be used as recording media.

List of references

1. Denisyuk. Yuri N, "On the reflection of optical properties of an object in a wave field of light scattered by it," *Doklady Akademii Nauk SSSR*, 144(6), pp. 1275–1278, 1962.
2. Burrow. G. M, and Gaylord. T. K, "Multi-beam interference advances and applications: nano-electronics, photonic crystals, metamaterials, subwavelength structures, optical trapping, and biomedical structures," *Micromachines, 2(2), pp. 221-257, 2011*.
3. Kuang. Z,Perrie. W, Leach. J, Sharp. M, Edwardson. S. P, Padgett. M, and Watkins. K. G, "High throughput diffractive multi-beam femtosecond laser processing using a spatial light modulator," *Appl. Surface Science, 255(5), pp. 2284-2289, 2008.*
4. Xie. X. S, Li. M, Guo. J, Liang. B, Wang. Z. X, Sinitskii. A, and Zhou. J. Y, "Phase manipulated multi-beam holographic lithography for tunable optical lattices," *Opt .Express. 15(11), 7032-7037, 2007.*
5. Kuang. Z, Perrie. W, Liu. D, Edwardson. S, Cheng. J, Dearden. G, and Watkins. K, "Diffractive multi-beam surface micro-processing using 10ps laser pulses," *Appl. Surface Science, 255(22), pp. 9040-9044, 2009.*
6. Gabor. D,"A new microscopic principle," *Nature, 161(4098), pp. 777-778, 1948.*
7. Gabor. Dionys, "Microscopy by reconstructed wave-fronts," *Proceedings of the Royal Society of London A: Mathematical, Physical and Engineering Sciences.*

The Royal Society, 197(1051), 1949.

8. Blanche. P. A, Bablumian, A., Voorakaranam, R., Christenson, C., Lin, W., Gu, T., and Peyghambarian, N. "Holographic three-dimensional telepresence using large-area photorefractive polymer," *Nature, 468(7320), pp. 80-83, 2010.*
9. Smalley. D. E., Smithwick. Q. Y. J., Bove. V. M., Barabas, J., and Jolly. S," Anisotropic leaky-mode modulator for holographic video displays," *Nature, 498(7454), pp. 313-317, 2013.*
10. Yamaji. M, Kawashima. H, Suzuki.J. I,and Tanaka. S, "Three dimensional micromachining inside a transparent material by single pulse femtosecond laser through a hologram," *Appl. Phys.Lett, 93*(4), *041116, 2008.*
11. Lai. S," Security holograms using an encoded reference wave," *Opt. Eng. 35(9), pp. 2470-2472, 1996.*
12. Millington, R. B., Mayes, A. G., Blyth, J., and Lowe, C. R, "A holographic sensor for proteases," *Analyt. Chem. 67(23), 4229-4233,1995.*
13. Yeh. S. L, and Lin. S. T, "Identifying a dot-matrix hologram by checking the intersecting angles of its gratings," *Opt. Comm. 283(2), pp. 243-248,2010.*
14. D. Xia, Z. Ku, S. C. Lee, and S. R. J. Brueck, "Nanostructures and functional materials fabricated by interferometric lithography," *Adv. Mater. 23(2), pp.147-149, 2010.*
15. "Security Hologram Labels and Stickers", 2015. Available: http://www.novavisioninc.com/pages/prd_hologram_holograms.html.
16. Makowski. M, Sypek. M, and Kolodziejczyk. A, "Colorful reconstructions from

a thin multi-plane phase hologram," *Opt. Express.16(15), pp. 11618-11622,2008.*

17. Dhar. L, Schnoes. M. G, Wysocki. T. L, Bair. H, Schilling.M, and Boyd. C, "Temperature-induced changes in photopolymer volume holograms," *Appl. Phys. Lett. 73(10), pp. 1337-1339, 1998.*
18. Kang. Y. H, Kim.K. H, and Lee. B, "Volume hologram scheme using optical fiber for spatial multiplexing," *Opt. Lett. 22(10), 739-741, 1997.*
19. Gao. H, Watson. J. M, Stuart. J. S, and Barbastathis. G, "Design of volume hologram filters for suppression of daytime sky brightness in artificial satellite detection," *Opt. Express, 21(5), pp. 6448-6458, 2013.*
20. Kostuk. R. K, Howlett. I. D, Gordon. M, Brownlee. J, de Leon. E, Orsinger. G, and Barton. J, "Degenerate Volume Holographic Imaging Techniques and Instruments for Subsurface Tissue Visualization," In *CLEO: Applications and Technology, pp. ATh1J-5,2015.*
21. "Holography", 2016. Available at: https://en.wikipedia.org/wiki/Holography.
22. Cooke. D. J, and Ward. A. A, "Reflection-hologram processing for high efficiency in silver-halide emulsions," *Appl.Opt.23(6), pp. 934-941, 1984.*
23. Tanaka. K, Kato. K, and Date. M, "Fabrication of holographic polymer dispersed liquid crystal (HPDLC) with high reflection efficiency," *Jap. Journal of Appl. Phys, 38(3A), L277,1999.*
24. Domschke. Angelika Maria, Xiaodong Hu, and Jian S. Zhou, "Reflection hologram sensor in contact lens," *U.S. Patent No. 7,927,519. 19, 2011.*
25. "Introduction to Volume Phase Holographic (VPH) Transmission Gratings and

Applications", available: http://www.kosi.com/na_en/products/holographic-gratings/.

26. Chang. C. T, and Bjorkstam. J. L, "Amplitude hologram efficiencies with arbitrary modulation depth, based upon a realistic photographic film model," *JOSA, 67(9), pp.1160-1164,1997.*
27. Samui. A. B, "Holographic recording medium," *Recent Patents on Materials Science, 1(1), pp.74-94, 2008.*
28. Callant. Paul R, and Jean-Marie O. Dewanckele, "Spectrally sensitized silver halide emulsions," *U.S. Patent No. 5,116,722. 26 May 1992.*
29. Gorin. Brian A, and Ping-Pei Ho, "Process for making high efficiency phase holograms," *U.S. Patent No. 4,510,221.9 Apr. 1985.*
30. Muller. Helmut, and Jorg. Gutjahr, "Stabilization of holograms formed in gelatin," *U.S. Patent No. 5,795,681. 18 Aug. 1998.*
31. Urabe. Shigeharu, and Shunichi. Aida, "Superfine grains," *U.S. Patent No. 5,196,300. 23 Mar. 1993.*
32. Kim, Jong-man, "Formed via pre-hardening silver halide emulsion, developing, bleaching, hardening, drying, fixing, treating with warm water, then drying again; optical recording material; light amplifiers," *U.S. Patent No. 6,811,930. 2 Nov. 2004.*
33. Crivello. J. V., and Reichmanis, E, "Photopolymer materials and processes for advanced technologies," *Chemistry of Materials, 26*(1), *pp. 533-548, 2013.*
34. "Radiation Chemistry in EB-and UV- Light-Cured Inks", 2000, September 27. Available:http://www.pcimag.com/articles/radiation-chemistry-in-eb-and-uv-light

-cured-inks.

35. Frederick. Haugh. Eugene, "Hologram recording in photopolymerizable layers." *U.S. Patent No. 3,658,526. 25 Apr. 1972.*

36. Trout. Torence J, Dominic M. Chan, and Bruce M. Monroe, "Mixture of fluorinated binder, unsaturated liquid monomer plasticizer, photoinitiator," *U.S. Patent No. 4,963,471. 16 Oct. 1990.*

37. Mikulchyk. T, Walshe. J, Cody. D, Martin. S, and Naydenova. I, "Humidity and temperature response of photopolymer-based holographic gratings," In *SPIE Optics Optoelectronics, International Society for Optics and Photonics, pp. 950809-950809, 2015.*

38. Robillard. Jean J, and Eric Chesak, "Holographic method and materials to detect and prevent forgery in identity cards," *U.S. Patent No. 5,835,245. 10 Nov. 1998.*

39. Lin. S. H, Cho. S. L, Chou. S. F, Lin. J. H, Lin. C. M, Chi. S, and Hsu. K. Y, "Volume polarization holographic recording in thick photopolymer for optical memory," *Opt. Express. 22(12), pp. 14944-14957, 2014.*

40. Akbari. H, Naydenova. I, and Martin. S, "Using acrylamide-based photopolymers for fabrication of holographic optical elements in solar energy applications," *Appl. Opt. 53(7), pp. 1343-1353, 2014.*

41. Frejlich. J. Photorefractive materials: fundamental concepts, holographic recording and materials characterization. *John Wiley & Sons, 2007.*

42. Günter, Peter, and Jean-Pierre Huignard, eds. Photorefractive materials and their applications. *Vol. 2. Berlin: Springer, 1989.*

43. "Photorefractive effect", 20th, October, 2013. available at: https://en.wikipedia.org/wiki/Photorefractive_effect.

44. Goonesekera. A, Wright. D, and Moerner. W. E, "Image amplification and novelty filtering with a photorefractive polymer," *Appl. Phys.Lett. 76(23), pp. 3358-3360, 2000.*

45. Blanche. P. A, Bablumian. A,Voorakaranam. R, Christenson. C, Lin, W. Gu. T, and Peyghambarian. N, "Holographic three-dimensional telepresence using large-area photorefractive polymer," *Nature, 468(7320), pp. 80-83,2010.*

46. Suzuki N, Tomita Y, Kojima T, "Holographic recording in TiO2 nanoparticle-dispersed methacrylate photopolymer films," *Appl. Phys. Lett. 81(22),pp. 4121-4123,2002.*

47. Suzuki N, and Tomita. Y, "Silica-nanoparticle-dispersed methacrylate photopolymers with net diffraction efficiency near 100%," *Appl. Opt.43(10), pp. 2125-2129, 2004.*

48. Lessard RA, and Bjelkhagen HI, "Practical holography XXI: Materials and Applications," *Proc SPIE. 6488: pp. 648-804, 2007.*

49. Saxby, G. Practical Holography, *3rd ed. Institute of Physics Publishing: UK, 2004.*

50. Bartolini. R, Hannan. W, Karlsons.D, and Lurie. M,"HOLOGRAPHY Embossed Hologram Motion Pictures for Television Playback," *Appl. Opt. 9(10), pp. 2283-2290, 1970.*

51. Tate. N, Naruse. M, Yatsui. T, Kawazoe. T, Hoga. M, Ohyagi. Y, and Ohtsu. M,

"Nanophotonic code embedded in embossed hologram for hierarchical information retrieval," *Opt. Express. 18(7), pp. 7497-7505, 2010.*

52. Butt. H, Montelongo. Y, Butler. T, Rajesekharan. R, Dai. Q, Shiva-Reddy. S. G, and Amaratunga. G. A, "Carbon nanotube based high resolution holograms," *Adv. Mater. 24(44), pp. OP331-OP336, 2012.*
53. Montelongo. Y, Tenorio-Pearl. J. O, Milne. W. I, and Wilkinson. T. D, "Polarization switchable diffraction based on subwavelength plasmonic nanoantennas," *Nano Lett. 14(1), pp.294-298, 2013.*
54. Cooper. D, Twitchett. A. C, Somodi. P. K, Midgley. P. A, Dunin-Borkowski. R. E, Farrer. I, and Ritchie, D. A, "Improvement in electron holographic phase images of focused-ion-beam-milled GaAs and Si PN junctions by in situ annealing," *Appl. Phys. Lett., 88(6), pp. 063510, 2006.*
55. Lasagni. A, Roch. T, Bieda. M, Benke. D, and Beyer. E, "High speed surface functionalization using direct laser interference patterning, breaking the 1 m2/min fabrication speed with sub-μm resolution," *In SPIE LASE International Society for Optics and Photonics, pp. 89680A-89680A, 2014.*
56. Lasagni. A. F, Acevedo. D. F, Barbero.C. A, and Mücklich. F, "One-Step Production of Organized Surface Architectures on Polymeric Materials by Direct Laser Interference Patterning," *Adv. Eng. Mater. 9(1-2), pp. 99-103,2007.*
57. Lasagni. A. F, Roch. T, Berger. J, Kunze. T, Lang. V,and Beyer. E, "To use or not to use (direct laser interference patterning), that is the question," *In SPIE LASE. International Society for Optics and Photonics, pp. 935115-935115, 2015.*

58. Zhai. T, Zhang. X, Pang. Z, and Dou. F, "Direct writing of polymer lasers using interference ablation," *Adv. Mater. 23(16), 1860-1864, 2011*.

59. Li. Y, Yamada. K, Ishizuka. T, Watanabe. W, Itoh. K, and Zhou. Z, "Single femtosecond pulse holography using polymethyl methacrylate," *Opt. Express, 10(21), pp. 1173-1178, 2002.*

60. Zhao. Q, Yetisen. A. K, Anthony. C. J, Fowler. W. R, Yun. S. H, and Butt. H," Printable ink holograms," *Appl. Phys. Lett. 107(4), pp. 041115, 2015.*

61. Menon. R, Gil. D, and Smith. H. I, "Experimental characterization of focusing by high-numerical-aperture zone plates," *JOSA A, 23(3), pp. 567-571, 2006.*

62. Deng. S, Yetisen. A. K, Jiang. K, and Butt. H," Computational modelling of a graphene Fresnel lens on different substrate," *RSC Adv. 4, pp. 30050-30058, 2014.*

63. Aieta. F, "Aberration-free ultrathin flat lenses and axicons at telecom wavelengths based on plasmonic metal surfaces," *Nano Lett.12, pp. 4932-4936, 2012.*

64. Kim. J. K, "Fabrication of micro Fresnel zone plate lens on a mode-expanded hybrid optical fiber using a femtosecond laser ablation system," *IEEE Photon. Tech. Lett. 21, pp. 21-25,2009.*

65. Morgan. B, Waits. C. M, Krizmanic. J, and Ghodssi. R, "Development of a deep silicon phase Fresnel lens using gray-scale lithography and deep reactive ion etching," *Microelectromech. Syst. 13, pp. 113-120,2004.*

66. Chao. W, Kim. J, Rekawa. S, Fischer. P, and Anderson. E. H," Demonstration of 12 nm resolution Fresnel zone plate lens based soft x-ray microscopy," *Opt. Exp.17, pp.17669-17677, 2009.*

67. "Zone Plate" , 2016. Available at: https://en.wikipedia.org/wiki/Zone_plate.

Appendix

Fabrication parameters of the Gratings.

Gold was evaporated over a microscopic glass to obtain a ~4.5 nm film with a transparency of~50%, and its absorption peak overlapped with the laser light used to produce the grating. Nd-Yttrium-Aluminum-Garnet pulsed laser (high-power compact Q-switched Nd:YAG oscillator with super Gaussian resonator, 700 mJ @ 1064 nm, 10 Hz) with a second harmonic generator, 350 mJ @ 532 nm 10 Hz, thermally stabilized with wavelength separation) was used to pattern gold. The parallel and radial surface gratings were patterned in line with Denisyuk reflection mode. A plane dielectric mirror was placed on a leveled surface, and an incident beam was aligned to be normal to the surface plane. The gold-coated substrate was placed over the mirror with a tilt angle of 5 ℉rom the surface plane of the mirror. The gold was patterned using 5 ns pulses (350mJ, 532 nm, 10 Hz, a spot size of~1 cm in diameter) of the Nd:YAG laser beam. The laser energy patterning the gold film was measured as ~10 mJ using a power meter. The radial gratings were created by replacing the plane mirror with a concave mirror, which had a diameter and radius of 2.5 and 6.2 cm, respectively.

Optical Characterisation.

The spectrometer (Ocean Optics) with an optical resolution of ~0.1-100 nm full width at half maximum was used to measure optical intensity with an integration time of 1 s to obtain the maximum peak intensity. COMSOL Multiphysics (v5.1) and MATLAB (Math Works, v8.1) were used for data processing and finite element simulations.

Realistic complex model

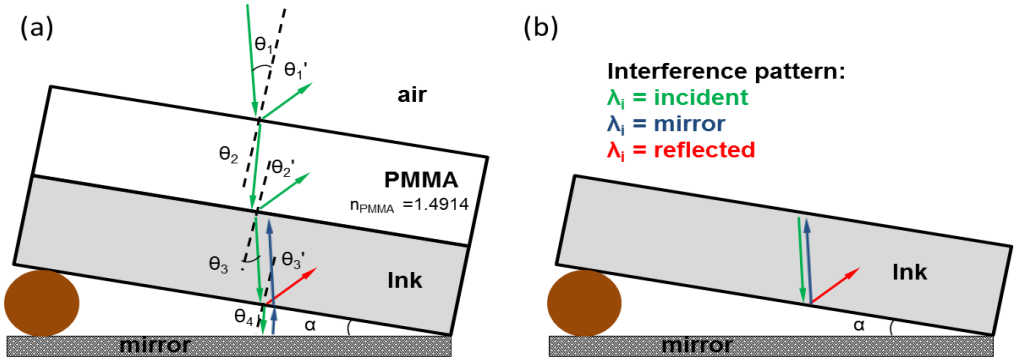

Figure A1 Schematic representation of the interference pattern created from (a) realistic complex phenomenon, (b) simplified model.

As mentioned in Chapter 5, the accurate model for interference of coherent beams is shown in Figure 1(a), it shows the realistic phenomenon of the internally reflected light from the ink-air interface. Additionally, the refractive index values need to be accounted more realistic estimations of the grating pattern. In model (b), we used a simplified model for this grating. The internal reflections play a small part in the profile of the interference pattern.